Available online at www.sciencedirect.com

ScienceDirect

Nuclear Physics A 973 (2018) 1–32

NUCLEAR PHYSICS A

www.elsevier.com/locate/nuclphysa

Cluster shell model: I. Structure of ^{9}Be, ^{9}B

V. Della Rocca [a,b], F. Iachello [b]

[a] *Gran Sasso Science Institute, viale Francesco Crispi 7, 67100 L'Aquila, Italy*
[b] *Center for Theoretical Physics, Sloane Laboratory, Yale University, New Haven, CT 06520-8120, USA*

Received 21 November 2017; received in revised form 13 February 2018; accepted 14 February 2018
Available online 24 February 2018

Abstract

We calculate energy spectra, electromagnetic transition rates, longitudinal and transverse electron scattering form factors and log ft values for beta decay in ^{9}Be, ^{9}B, within the framework of a cluster shell model. By comparing with experimental data, we find strong evidence for the structure of these nuclei to be two α-particles in a dumbbell configuration with Z_2 symmetry, plus an additional nucleon.

Keywords: Cluster model; Alpha-cluster nuclei; Cluster shell-model

1. Introduction

Recently, we have introduced [1] a cluster shell model (CSM) and studied the single particle levels in cluster potentials with Z_2, D_{3h}, and T_d symmetry, appropriate to ^{8}Be, ^{12}C, and ^{16}O respectively. In this article, we begin a systematic application of the CSM to the structure of light nuclei by performing a calculation of the nuclei ^{9}Be and ^{9}B. These nuclei are the simplest nuclei within CSM, since the cluster field has Z_2 symmetry which preserves both axial symmetry and reflection symmetry on a plane perpendicular to the symmetry-z-axis, and thus the intrinsic states can be labeled by K^P where K is the projection of the angular momentum on the symmetry axis and P the parity.

E-mail addresses: valeria.dellarocca@gssi.it, valeria.dellarocca@yale.edu (V. Della Rocca), francesco.iachello@yale.edu (F. Iachello).

https://doi.org/10.1016/j.nuclphysa.2018.02.003
0375-9474/

Another important reason is that these nuclei have been extensively investigated in the past both from the cluster point of view [2–4] culminating in the extensive work of Okabe, Abe and Tanaka [5–7] using the Linear Combination of Atomic Orbitals (LCAO), and from that of the spherical [8] and deformed [9] shell model. In recent years, Fermion Molecular Dynamics (FMD) [10–13] and Antisymmetric Molecular Dynamics (AMD) [14–16] have provided very detailed and accurate descriptions of the Be isotopes both even and odd. In another seminal development, von Oertzen [17–20] has discussed the structure of ^{9}B, ^{9}Be in a two-center shell model, in which these nuclei are seen as ^{8}Be+one proton (or neutron). In yet another seminal development, Descouvemont and others [21–29] have calculated properties of ^{9}Be, ^{9}B in a three-body cluster model, in which the three-body dynamics is fully taken into account. This work is particularly important since in the 3-body cluster model one can calculate both the energy and the width of the unbound states. Our point of view is identical to that of these references. Indeed it is a simplified version of the LCAO method and of the 3-body model, which however has the advantage of producing in most part analytical and transparent results which can be easily compared with experiment.

Finally, the structure of these light nuclei has been the subject of several investigations in very recent years, within the framework of ab initio calculations, both with quantum Monte Carlo methods (GFMC) [30–34] and with no core shell-model methods (NCCI) [35–38]. Our approach is meant to provide a benchmark for comparison with these calculations. Our main interest is to see how cluster features emerge from fully microscopic ab-initio calculations.

The paper is organized as follows. In Sect. 2, we briefly review the structure of ^{8}Be which generates the field in which the single particle moves. In Sect. 3, we show the single-particle levels, ϵ_Ω, and intrinsic wave functions, χ_Ω, appropriate to clusters with Z_2 symmetry. In Sect. 3.1, we describe the spectra built on top of these intrinsic states, evaluating the moments of inertia and decoupling parameters. Since the intrinsic states have axial symmetry, our approach here is similar to that of the Nilsson model [39], with the difference that we are also including $\lambda > 2$ multipoles. In Sect. 3.4, we describe how to calculate electromagnetic transition rates, and magnetic and electric moments, and compare with experimental data. In Sect. 3.6 we describe how to calculate form factors in electron scattering and compare with data. In Sect. 4, we describe how to calculate log ft values for beta decay. In Sect. 5, we describe how the structure of ^{9}B is modified by the Coulomb interaction.

Our conclusion, Sect. 6, is that clustering survives the addition of one particle, and even enhances it. Indeed, as already remarked by von Oertzen years ago [17–20], the odd neutron in ^{9}Be provides binding of this nucleus relative to ^{8}Be in a way very similar to π-binding in molecules [40].

The strongest evidence for the persistence of clustering in the odd nuclei ^{9}Be, ^{9}B is provided by electromagnetic rates and form factors in electron scattering, especially the $B(E2)$ values along the ground state band with $K^P = 3/2^-$ and the electric elastic and inelastic form factors.

2. Structure of ^{8}Be

A prerequisite for studying ^{9}Be and ^{9}B in the CSM is the choice of the cluster potential in which the particles move. This potential is determined by the structure of ^{8}Be. We assume that ^{8}Be is composed of two α-particles in a dumbbell configuration. Each α-particle is assumed to have a gaussian matter and charge distribution $\rho_\alpha(\vec{r})$ given by

$$\rho_\alpha(\vec{r}) = \left(\frac{\alpha}{\pi}\right)^{3/2} e^{-\alpha r^2} \tag{1}$$

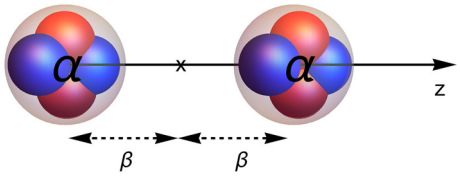

Fig. 1. Dumbbell configuration of ^{8}Be.

and is located at a distance β from the center of mass, Fig. 1. The normalized matter and charge distributions are obtained by multiplying Eq. (1) by 4 and 2 respectively. The value of α as obtained from electron scattering in ^{4}He is $\alpha = 0.56$ fm^{-2} [41]. The matter and charge density of the dumbbell configuration is then [1]

$$\begin{aligned}\rho(\vec{r}) &= \left(\frac{\alpha}{\pi}\right)^{3/2} \sum_{i=1}^{2} \exp\left[-\alpha\,(\vec{r}-\vec{r}_i)^2\right] \\ &= \left(\frac{\alpha}{\pi}\right)^{3/2} e^{-\alpha(r^2+\beta^2)} 4\pi \sum_{\lambda} i_\lambda(2\alpha\beta r) \left(\frac{2\lambda+1}{4\pi}\right) [1+P_\lambda(-1)]\, P_\lambda(\cos\theta)\end{aligned} \tag{2}$$

where $i_\lambda(x) = j_\lambda(ix)/i^\lambda$ is the modified spherical Bessel function.

Properties of this configuration can be obtained in a variety of ways, either by solving the Schrodinger equation with a Morse-type [42] or a Volkov-type [43] potential or by making use of the algebraic cluster model, ACM, [44–47], which is an application to cluster structures of the algebraic theory of molecules [48].

2.1. Energy spectrum

The energy spectrum is given approximatively by

$$E(v,L) = E_0 + D\left(v+\frac{1}{2}\right) + BL(L+1) \tag{3}$$

where $v = 0, 1, \ldots$ is the vibrational quantum number and $B = \frac{\hbar^2}{2\mathscr{I}}$ the inertia parameter. The three components of the moment of inertia $\mathscr{I}$ can be evaluated to be

$$\begin{aligned}\mathscr{I}_x &= Am\beta^2 + \frac{Am}{\alpha} \\ \mathscr{I}_y &= Am\beta^2 + \frac{Am}{\alpha} \\ \mathscr{I}_z &= \frac{Am}{\alpha}\end{aligned} \tag{4}$$

for a gaussian distribution, which reduce to $\mathscr{I}_x = \mathscr{I}_y = Am\beta^2$, $\mathscr{I}_z = 0$ for point particles. In Eq. (4), $A = 8$, and m is the nucleon mass. For the case in which $\mathscr{I}_x = \mathscr{I}_y = \mathscr{I}$ and $\mathscr{I}_z \neq 0$, as in Eq. 4, Eq. (3) becomes

$$E(v,L) = E_0 + D\left(v+\frac{1}{2}\right) + BL(L+1) - (B_x - B_z)K^2 \tag{5}$$

which is the energy formula of the symmetric top [49]. In Eq. (4), $B_x = \hbar^2/(2\mathscr{I}_x) = B_y$ and $B_z = \hbar^2/(2\mathscr{I}_z)$. For ^{8}Be, $K = 0$, and Eq. (5) reduces to Eq. (3).

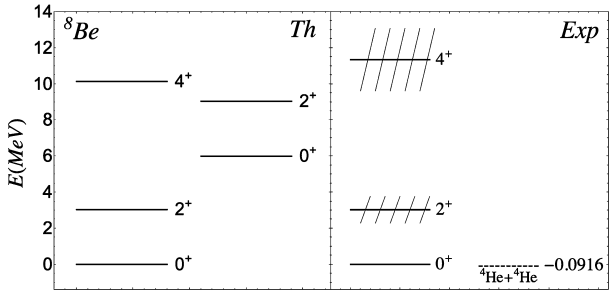

Fig. 2. Comparison between the cluster spectrum and the experimental spectrum [50] of ^{8}Be. In panel (a), $D = 6$ MeV, $B = 0.507$ MeV. The dashed region is given by the width, Γ, of the states [50].

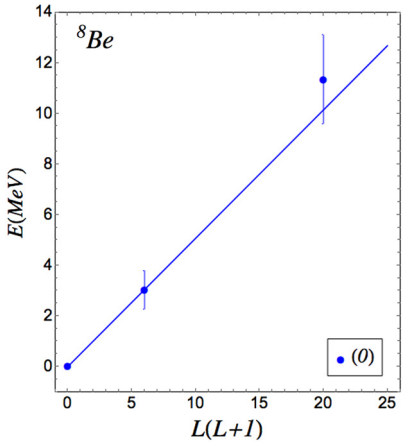

Fig. 3. Observed cluster rotational band in ^{8}B, $v = 0$. The theoretical line is given by Eq. (3) with $B = 0.507$ MeV. The experimental bar is the width Γ.

The spectrum, Eq. (3), is compared with the experimental spectrum in Fig. 2. One can see the occurrence of a ground rotational band, Fig. 3. The inertia parameter $B = \frac{\hbar^2}{2\mathscr{I}}$ extracted from the energy difference $E_{2^+} - E_{0^+}$ is $B = 0.507$ MeV, from which one obtains $\mathscr{I}/m = 40.8$ fm^2 and $\beta = 1.82$ fm. We estimate the error in this extraction to be 4%, giving $\beta = 1.82(8)$ fm. From the values of α and β one can also calculate the charge and matter radius given by the expression

$$\langle r^2 \rangle^{1/2} = \sqrt{\frac{3}{2\alpha} + \beta^2} \tag{6}$$

One obtains $\langle r^2 \rangle^{1/2} = 2.45$ fm.

No evidence for vibrational bands is reported in [50], although Barker [51] suggested in the 1960s one such a band at $E_x \sim 6$ MeV, in accordance to similar vibrational bands observed in ^{12}C and ^{16}O. All states in Fig. 2 are unbound as indicated by the dash in the experimental spectra, but we will treat them as bound states as long as their width is much smaller than their excitation energy. This is not the case for the vibrational state which is then deleted from consideration. With the value of $\beta = 1.82$ fm, we obtain the charge and matter distribution of ^{8}Be shown in Fig. 4.

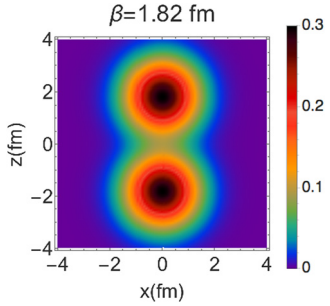

Fig. 4. Charge and matter distribution of ^{8}Be. The color code is in fm^{-3}.

Table 1
Electromagnetic transition rates, and energies, in ^{8}Be. $B(EL)$ values in e^{2}fm^{2L} and E (keV) $= 507L(L+1)$. The experimental value of $B(E2; 2^+ \to 0^+)$ is estimated from [52] using GFMC.

$B(EL; L^P \to 0^+)$	Th	(Exp)	$E(L^P)$	Th	Exp
$B(E2; 2^+ \to 0^+)$	14.0	(21.0(23))	$E(2^+)$	3060	3030
$B(E4; 4^+ \to 0^+)$	153.3		$E(4^+)$	10200	11350

2.2. Electromagnetic transition rates

Electromagnetic transition rates along a rotational band belonging to a given vibrational state, v, can be obtained analytically within the framework of the algebraic cluster model [44–46] and are given by

$$B(EL; 0 \to L) = \left(\frac{Ze\beta^L}{2}\right)^2 \left(\frac{2L+1}{4\pi}\right) [2 + 2P_L(-1)]\,. \tag{7}$$

Here $Z = 4$ and P_L is a Legendre polynomial. Inserting the value $\beta = 1.82$ fm one obtains the results of Table 1. Note that Eq. (7) includes all multipoles $2, 4, 6, \ldots$. Because of the cluster structure all multipoles are enhanced. This is in contrast with a purely quadrupole deformation where only $\lambda = 2$ is enhanced and is the main difference between a quadrupole structure and a cluster structure.

No experimental value is available for $B(E2; 2^+ \to 0^+)$ and $B(E4; 4^+ \to 0^+)$. Daker et al. [52] have made a model dependent estimate from radiative capture using GFMC. This value is shown in Table 1 in parenthesis and it is in fair agreement with our calculated value.

From Eq. (7), one can also calculate

$$B(E2; L-2 \to L) = \left(Ze\beta^2\right)^2 \left(\frac{5}{4\pi}\right) \langle L-2, 0, 2, 0|L, 0\rangle^2 \tag{8}$$

and the quadrupole moments

$$Q^{(2)}(L) = \sqrt{\frac{16\pi}{5}} \left(Ze\beta^2\right) \sqrt{\frac{5}{4\pi}} \langle L, 0, 2, 0|L, 0\rangle \langle L, L, 2, 0|L, L\rangle \tag{9}$$

These are shown in Table 2, for $\beta = 1.82$ fm.

We note here that the estimated $B(E2)$ values and quadrupole moment are better fit with $\beta = 2.0$ fm. However, the experimental $B(EL)$ values reported in Ref. [52] are model dependent.

Table 2
Deduced electromagnetic properties in ^{8}Be. $B(E2)$ values in e^2fm^{2L} and quadrupole moments in efm^2. The experimental values in parenthesis are estimated from [52].

	Th	(Exp)
$B(E2; 4^+ \to 2^+)$	20.0	(27.2(15))
$Q(2^+)$	−7.6	(−9.1(2))

Table 3
Comparison of inertial parameters, B, with ab initio calculations. CSM value is fitted to experiment. NCCI values extracted from [38]. All values in MeV.

	GFMC [32]		NCCI [38]		CSM	Exp
	AV18	AV18/IL2	JISP16	NNLO		
B (MeV)	0.433(66)	0.683(50)	0.627	0.599	0.507	0.507

We will therefore assume, in the following sections, a value of $\beta = 1.82$ fm. This value is in remarkable agreement with the value $\beta = 1.77$ fm extracted from Fig. 3 of [6] which represents the result of the microscopic LCAO method.

2.3. Form factors

Form factors can also be calculated analytically within the framework of the algebraic cluster model [44–46] and are given by

$$\begin{aligned} F_L(0 \to L; q) &= c_L\, j_l(q\beta) e^{-q^2/4\alpha} \\ c_L^2 &= \frac{2L+1}{4}\,[2 + 2P_L(-1)]\,, \end{aligned} \tag{10}$$

where $j_l(q\beta)$ is the spherical Bessel function and q the momentum transfer. Since ^{8}Be is unstable they cannot be measured. However, Eq. (10) will play a major role in subsequent sections when dealing with ^{9}Be.

2.4. Comparison with ab initio and with phenomenological shell model calculations

Extensive calculations have been performed for ^{8}Be. We compare here first with recent ab initio calculations using quantum Monte Carlo methods [30–32] and no-core shell model [35–38]. The results of these calculations depend on the interaction. All calculations produce a rotational band with energy given by Eq. (3). The crucial quantity is the inertia parameter B. In Table 3 we show a comparison between the calculated and experimental inertia parameter for some of the calculations. It appears that the ab-initio values are in fair (GFMC) or good (CSSI) agreement with experiment.

Another quantity of interest is the $B(E2; 2_1^+ \to 0_1^+)$. In Table 4 we show a comparison between the calculated values and those estimated from [32] using GFMC. No statement can be made here, except for the fact that the NCCI results have not yet converged to the estimated value. A similar conclusion can be drawn for the radii. The r.m.s. value calculated in CSM is

Table 4
Comparison of $B(E2; 2_1^+ \rightarrow 0_1^+)$ values with ab initio calculations. Experimental value, in parenthesis, estimated from [52] using GFMC. The not-yet converged NCCI value is extracted from Fig. 2 of [38] at $\hbar\omega = 20$ MeV and $N_{max} = 10$. All values in e^2fm^4.

	GFMC [32]	NCCI [38]	CSM	(Exp)
$B(E2; 2_1^+ \rightarrow 0_1^+)$	21.0(23)	8.0	14.0	(21.0(23))

$\langle r^2 \rangle^{1/2} = 2.45$ fm. The r.m.s. value in CSSI is ~ 1.9 fm [38] but as one can see from Fig. 2 of [38] it is not yet converged.

Phenomenological shell model calculations of ^{8}Be were performed long ago [8]. Also these calculations produce a rotational band with inertial parameter $B = (0.640 - 0.587)$ MeV, depending on the interaction.

In summary, all calculations give rise to the rotational structure of Fig. 2, with moment of inertia parameters in the range $B = (0.4 - 0.6)$ MeV. For shell model calculations in which particles occupy the $1p$-level [8], this result can be traced to the fact that the spherical $1p$ single-particle level forms the fundamental representation of $SU(3)$, Elliott model [53], and therefore $SU(3)$ symmetry, which produces energy levels which go as $L(L+1)$, is a good symmetry.

3. Structure of ^{9}Be

We assume that ^{9}Be is composed of a neutron moving in the field of a ^{8}Be core with Z_2 symmetry. The single particle levels, ϵ_Ω, and wave functions, χ_Ω, are obtained by the method of [1]. We use here $V_0 = 20$ MeV, $V_{0,so} = 22$ MeVfm^2 and $\alpha = 0.1115$ fm^{-2} obtaining the single particle energies of Fig. 5. Due to the symmetry of the system, the projection K of the angular momentum along the symmetry axis and the parity P are good quantum numbers and states can be labeled by K^P, or by the equivalent molecular notation, as in Fig. 5. At $\beta = 1.82$ fm, the two lowest levels are occupied and the odd-neutron can be in any of the three levels $K^P = 3/2^-[1\pi_u 3/2]$, $K^P = 1/2^-[1\pi_u 1/2]$ and $K^P = 1/2^+[2\sigma_g 1/2]$, where we are using the notation of [1]. The intrinsic energies ϵ_Ω of these states are given in Table 5. The level $3/2^-$ is bound, while $1/2^-$, $1/2^+$ are not. The corresponding intrinsic wave functions are [1]:

$$|\chi_\Omega\rangle = \sum_{nljm} c^\Omega_{nljm} |n \frac{1}{2} ljm\rangle, \tag{11}$$

where Ω labels the states and where the expansion coefficients are evaluated in $\beta = 1.82$ fm. For the case discussed here $\Omega \equiv K^P$.

Although the odd particle could polarize the core and this would lead to a different equilibrium value β_K for each K, we assume here that β_K is independent of K, i.e. a rigid core. Values of β_K extracted from Fig. 3 of [6] are $\beta_{^8\mathrm{Be}} = 1.77(8)$ fm, $\beta_{3/2^-} = 1.65(8)$ fm, $\beta_{1/2^-} = 1.65(8)$ fm, $\beta_{1/2^+} = 2.17(11)$ fm. The polarization effect $\beta_{^9\mathrm{Be}} - \beta_{^8\mathrm{Be}}$ in [6] is $-0.12(10)$ fm for $3/2^-$ and $1/2^-$ and $+0.40(19)$ fm for $1/2^+$. However, these values come from the interplay of the core contribution and the single particle contribution. We explicitly include the single particle contribution as shown in the following subsections and obtain good values of the moments of inertia and decoupling parameters. We therefore feel that our assumption is good, especially for the $K^P = 3/2^-$ and $K^P = 1/2^-$ levels. For the $K^P = 1/2^+$ level the assumption is only fair, as one can see also from the flat behavior as a function of β of this level, $2\sigma_g 1/2$ in molecular

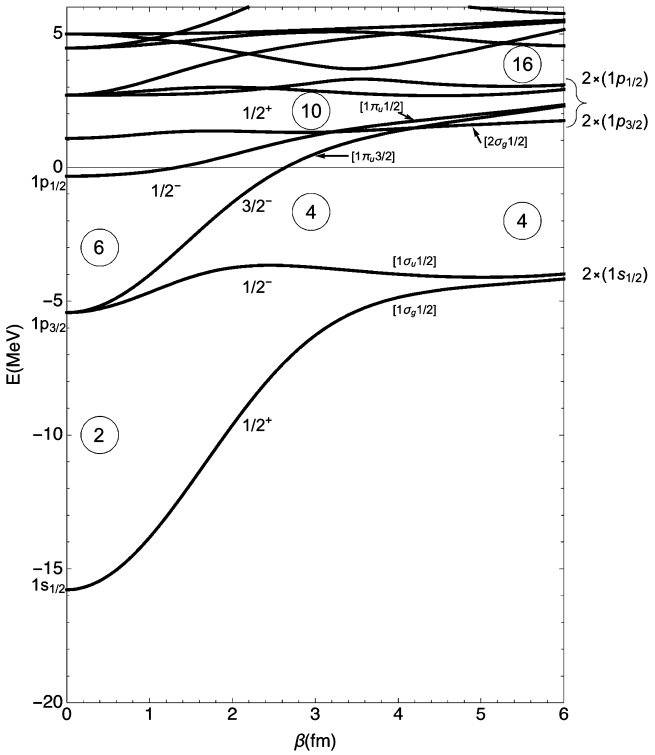

Fig. 5. Energy levels ϵ_Ω in a potential with $V_0 = 20$ MeV, $V_{so} = 22$ MeVfm^2 and $\alpha = 0.1115$ fm^{-2}, appropriate to ^{9}Be.

Table 5
Intrinsic energies in ^{9}Be at $\beta = 1.82$ fm.

State $\Omega \equiv K^P$	ϵ_Ω (MeV)
$3/2^-$	-1.78
$1/2^-$	$+0.32$
$1/2^+$	$+1.35$

notation, in Fig. 5. This level may not even be a resonance but rather a virtual state, as pointed out in [24,29]. Also, more levels could be included, and the core could be broken by promoting neutrons from the core to the valence space. We take here an inert core and a valence space consisting of only the three levels in Table 5. Effects of taking β_K different for each K can be easily studied in the CSM approach since our wave functions, Eq. (11), depend on β, and have been evaluated for any value of β in the range 0–6 fm. In the majority of cases, the study can be done by simple scaling considerations, since our results are given by explicit analytic formulas.

3.1. Energy spectra

Energy spectra are obtained as in the collective model [39]. On each single particle level of ϵ_K there is built a rotational band, with $J = K, K+1, K+2, \ldots$. The energy levels of each band are described by [56].

Table 6
The three components of the moment of inertia, $\mathscr{I}^n/m$, due to the odd neutron and of the total moment of inertia $\mathscr{I}/m$. All values in fm^2.

K^P	$3/2^-$	$1/2^-$	$1/2^+$
$\mathscr{I}^n_x/m$	6.1	8.4	12.6
$\mathscr{I}^n_y/m$	6.1	8.4	12.6
$\mathscr{I}^n_z/m$	8.0	8.2	11.6
$\mathscr{I}_x/m$	46.9	49.2	53.4
$\mathscr{I}_y/m$	46.9	49.2	53.4
$\mathscr{I}_z/m$	22.3	22.5	25.9

$$E(J,K) = \epsilon_K + \frac{(\hbar)^2}{2\mathscr{I}}\left[J(J+1) - K^2 + \delta_{(K,1/2)}a(-)^{J+1/2}(J+1/2)\right] \tag{12}$$

The term $-K^2$ is often omitted, but it is kept here because of importance when several K values are considered. The energy levels depend on the moment of inertia, $\mathscr{I}$, and on the so-called decoupling parameter, a, equal to [57]

$$a = -\sum_{nlj}(-)^{j+(1/2)}\left(j+\frac{1}{2}\right)|c^{1/2}_{nlj}|^2 \tag{13}$$

The decoupling parameter contributes only to $K = 1/2$ bands, see Eq. (12). Since the diagonalization procedure of [1] gives the coefficients $c^{1/2}_{nlj}$ for each $K = 1/2$ state, we can evaluate the decoupling parameters by means of Eq. (13)

$$a(1/2^-) = 0.77 \qquad , \qquad a(1/2^+) = 1.48. \tag{14}$$

The moment of inertia $\mathscr{I}$ in ^{9}Be can be obtained by adding the contribution of the odd neutron, $\mathscr{I}^n$, to that of the ^{8}Be core, $\mathscr{I}^c$, previously determined in Sect. 2. The assumption here is that the odd neutron is dragged along in a rigid fashion. As discussed in [56] this assumption may not be good but it is used here to conform with practice in the collective model.

The odd particle contribution to the three components $\mathscr{I}_x$, $\mathscr{I}_y$, $\mathscr{I}_z$ can be calculated as

$$\begin{aligned}
\mathscr{I}^n_x &= m\int (y^2+z^2)|\chi_\Omega|^2 d^3\vec{r} \\
\mathscr{I}^n_y &= m\int (x^2+z^2)|\chi_\Omega|^2 d^3\vec{r} \\
\mathscr{I}^n_z &= m\int (x^2+y^2)|\chi_\Omega|^2 d^3\vec{r},
\end{aligned} \tag{15}$$

where m is the nucleon mass, and χ_Ω is the intrinsic wave function of Eq. (11). For the three single particle levels we obtain the values given in Table 6.

Adding the total moment of inertia of the core, we obtain the total moment of inertia,

$$\mathscr{I} = \mathscr{I}^c + \mathscr{I}^n \tag{16}$$

also given in Table 6.

In addition to the moments of inertia one can also calculate the charge and matter radii. In the approximation used in this paper, the charge radius $\langle r^2\rangle^{1/2}_{\text{charge}}$ in ^{9}Be is the same as in ^{8}Be

Table 7
Radii of the states K^P in ^{9}Be at $\beta = 1.82$ fm.

K^P	$\langle r^2\rangle_n^{1/2}$ (fm)	$\langle r^2\rangle_{matter}^{1/2}$ (fm)
$3/2^-$	3.53	2.59
$1/2^-$	4.19	2.70
$1/2^+$	5.16	2.88

and given by $\langle r^2\rangle_{\text{charge}}^{1/2} = 2.45(10)$ fm, with an estimated error of 4%. The experimental value deduced by Bergstrom et al. [54] is $\langle r^2\rangle_{\text{charge}}^{1/2} = 2.46(11)$ fm, in excellent agreement with the calculated value. It should be noted that two contributions play a role in an accurate calculation of charge radii, the proton r.m.s. radius $\langle r^2\rangle^{1/2} = 0.87$ fm and the center of mass (recoil) effect [55]. The former contribution vanishes when considering the difference $\langle r^2\rangle_{^9\text{Be}}^{1/2} - \langle r^2\rangle_{^8\text{Be}}^{1/2}$. The latter contribution is estimated to be of order $1/A^2 \sim 0.01$, since it is the cancellation of several terms. This is within our estimated error. The matter radius $\langle r^2\rangle_{\text{matter}}^{1/2}$ is obtained by adding the cluster density to the odd-neutron matter density, yielding

$$\langle r^2\rangle_{matter} = \left[A\langle r^2\rangle_c + \langle r^2\rangle_n\right]\frac{1}{A+1} \tag{17}$$

where $A = 8$ is the mass number of the cluster and $\langle r^2\rangle_c^{1/2} = 2.45$ fm.

The odd particle contribution can be calculated as

$$\langle r^2\rangle_n = \int r^2|\chi_\Omega|^2 d^3\vec{r} \tag{18}$$

The corresponding r.m.s. radius of the three intrinsic states of Table 5 is given in Table 7. Adding the cluster contribution as in (17), one obtains the matter radii given in the right hand side of Table 7.

The matter distribution is also shown in Fig. 6 to be compared with the NCCI calculations, as reported in Fig. 5 of [37]. The CSM matter distribution is somewhat more extended than the NCCI matter distribution. The matter distribution is instead in perfect agreement with the results of the LCAO method, as shown in Fig. 10 of [6].

As discussed in Sect. 2, for a situation in which $\mathscr{I}_z \neq 0$ and $\mathscr{I}_x = \mathscr{I}_y = \mathscr{I}$, one should use a more general form for the rotational energy. In the present case, the formula is

$$\begin{aligned} E(J,K)_{rot} = &\frac{\hbar^2}{2\mathscr{I}}[J(J+1) - 2K^2 + \delta_{K,1/2}a(-)^{J+1/2}(J+1/2)] + \\ &+ \frac{\hbar^2}{2\mathscr{I}}\left(\frac{\mathscr{I}}{\mathscr{I}_z} - 1\right)K^2, \end{aligned} \tag{19}$$

where the terms $2K^2$ and a arise from Coriolis coupling [57] and the last term from $\mathscr{I}_z \neq 0$. It turns out that for the situation described here $(\frac{\mathscr{I}}{\mathscr{I}_z} - 1) \sim 1$ and therefore Eq. (19) reduces approximately to Eq. (12), which is then the formula we use in analyzing experimental data.

Using the values of ϵ_K, $\mathscr{I}$ and a, and Eq. (12) we then calculate the energies $E(J,K)$. The values so obtained are shown in Table 8 and in Figs. 7 and 8 where they are compared with experiment. One can see here an excellent agreement for the rotational bands, and a good agreement for the intrinsic energies. The three expected cluster states $K^P = 3/2^-[1\pi_u 3/2]$, $K^P = 1/2^-[1\pi_u 1/2]$, and $K^P = 1/2^+[1\sigma_g 1/2]$ are all observed, the only discrepancy being

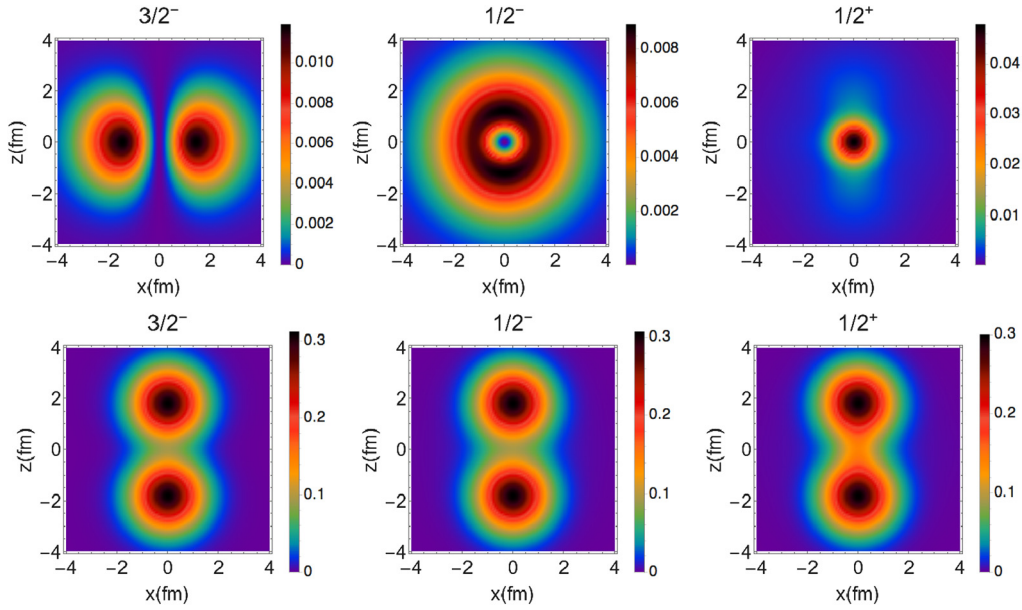

Fig. 6. Neutron density (top) and matter density (bottom) at $\beta = 1.82$ fm. Note the different color scale of top and bottom panels. The color code is in fm^{-3}.

Table 8
Calculated energy levels in ^{9}Be. All units in MeV.

$K^P = 3/2^-$	$K^P = 1/2^-$	$K^P = 1/2^+$
$E_{3/2^-} = 0$	$E_{1/2^-} = 1.3$	$E_{1/2^+} = 2.1$
$E_{5/2^-} = 2.2$	$E_{3/2^-} = 3.6$	$E_{3/2^+} = 5.0$
$E_{7/2^-} = 5.3$	$E_{5/2^-} = 4.0$	$E_{5/2^+} = 4.0$
$E_{9/2^-} = 9.3$	$E_{7/2^-} = 9.3$	$E_{7/2^+} = 10.8$
$E_{11/2^-} = 14.1$	$E_{9/2^-} = 10.1$	$E_{9/2^+} = 9.1$

Table 9
Inertia parameters and decoupling parameters in ^{9}Be.

^{9}Be	B (MeV)		a	
	Exp	Calc	Exp	Calc
$K^P = 3/2^-$	0.486(24)	0.441		
$K^P = 1/2^+$	0.385(19)	0.387	1.61(8)	1.48
$K^P = 1/2^-$	0.542(54)	0.420	0.89(9)	0.77

that the $K^P = 1/2^+$ is observed to be about 1 MeV lower than calculated. The agreement is very remarkable in view of the fact that there are no free parameters that have been adjusted, the value of β having been fixed from the moment of inertia of ^{8}Be. A summary of inertial parameters and decoupling parameters in ^{9}Be is given in Table 9.

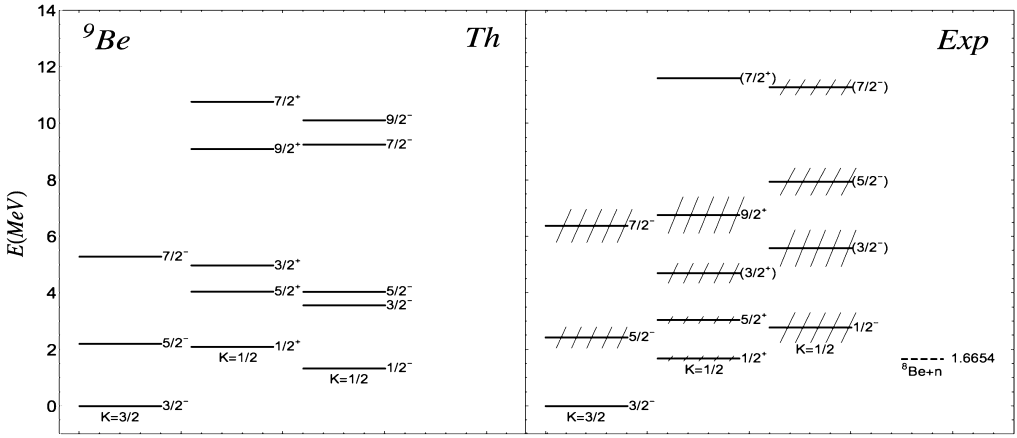

Fig. 7. Comparison between the cluster spectrum in CSM and the experimental spectrum of ^{9}Be [50]. The dashed region is given by the width of the states.

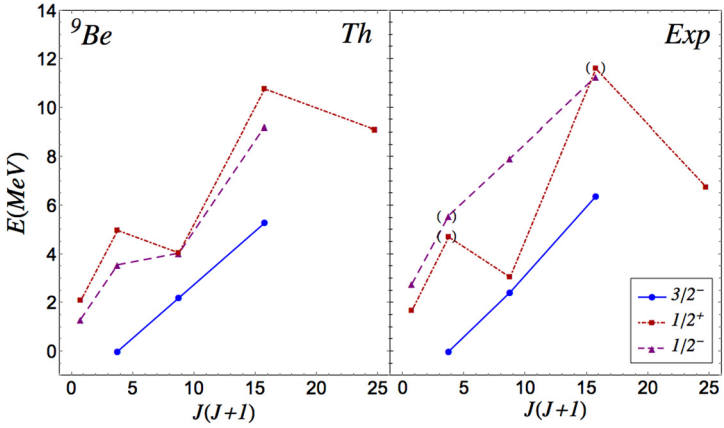

Fig. 8. Observed rotational bands in ^{9}Be.

3.2. Comparison with ab initio calculations

Energy levels in ^{9}Be have been calculated both in GFMC [34] and in NCCI [38]. From the calculated energies one can extract inertial, B, and decoupling parameters, a. A comparison with CSM results is shown in Table 10. From this table and from Table 9 one can see that all calculations are qualitatively in agreement with each other and with experiment. However, quantitatively discrepancies occur, especially for NCCI. The value of B for $K^P = 3/2^-$ in GFMC is instead in excellent agreement with experiment. It would be of interest to see how the calculated values for $K^P = 1/2^+, 1/2^-$ in GFMC compare with experiment.

In the case of NCCI it is also possible to compare the intrinsic energies ϵ_K of ^{9}Be relative to ^{8}Be. This comparison is shown in Table 11. It is interesting to note that both CSM and NCCI have the state $K^P = 3/2^-$ bound and the states $K^P = 1/2^+, 1/2^-$ unbound, although the energies of these states in NCCI are much higher than in CSM and in experiment.

Table 10
Comparison of ab-initio and CSM values of the inertial parameter B and the decoupling parameter a. GFMC extracted from [34] and NSSI extracted from [38].

K^P	B (MeV)				a			
	GFMC	NCCI		CSM	GFMC	NCCI		CSM
		NNLO	JISP			NNLO	JISP	
$3/2^-$	0.480	0.582	0.627	0.441				
$1/2^+$	–	0.356	0.397	0.387	–	2.43	2.12	1.48
$1/2^-$	–	0.582	0.620	0.420	–	0.25	0.44	0.77

Table 11
Comparison of intrinsic energies of ^{9}Be relative to ^{8}Be. The NCCI values are extracted from [38].

K^P	ϵ_K (MeV)		
	NCCI		CSM
	NNLO	JISP	
$3/2^-$	−2.27	−3.70	−1.78
$1/2^+$	3.46	3.26	1.35
$1/2^-$	5.25	4.12	0.32

Table 12
Comparison of LCAO, 3-body cluster and CSM values of the intrinsic parameter B and decoupling parameter a.

K^P	B (MeV)		
	LCAO [7]	3-BODY [22]	CSM
$3/2^-$	0.414	0.454	0.441
$1/2^+$	0.223	0.246	0.387
$1/2^-$	0.329	0.643	0.420
K^P	a		
	LCAO [7]	3-BODY [22]	CSM
$1/2^+$	2.65	2.07	1.48
$1/2^-$	0.76	−0.12	0.77

3.3. Comparison with LCAO and 3-body cluster

Results of LCAO [5–7] and 3-body cluster [21–29] depend on the details of the interaction and method. We compare here the values of B and a extracted from Fig. 4 of [7] and of Table III of [22]. The comparison in shown in Table 12. Similarly, one can compare the intrinsic energies extracted from Fig. 4 of [7] and Table III of [22] by removing the rotational contribution. The comparison in shown in Table 13. The agreement between these calculations with the CSM is very good, a remarkable result since the CSM has only one parameter β which has been fixed by the moment of inertia of ^{8}Be. The comparison between other calculations and CSM has been done in Tables 10–13 for the intrinsic energies, ϵ_K, the inertial parameter, B, and the decoupling parameter, a, which are the quantities of interest in this paper. It should be noted however that

Table 13
Comparison of intrinsic energies of ^{9}Be relative to ^{8}Be for LCAO, 3-body, and CSM.

K^P	ϵ_K (MeV)		
	LCAO [7]	3-BODY [22]	CSM
$3/2^-$	−0.62	−0.68	−1.78
$1/2^+$	3.17	2.85	1.35
$1/2^-$	2.81	2.23	0.32

the calculations reported in [22] and enlarged in [24] provide a more accurate overall description of energies, in addition to a description of widths not attempted here.

3.4. Electromagnetic transitions

Electromagnetic transition rates are obtained as in the collective model. The wave functions are factorized as a product of the intrinsic wave functions, χ_Ω, previously obtained [1], the vibrational functions of the cluster ψ_{vib} which depend on the vibrational quantum number v of Eq. (3), and a rotational part which we take as that of the symmetric top, that is

$$|\Omega, IMK\rangle = \sqrt{\frac{2I+1}{16\pi^2}}\psi_{vib}\left\{\chi_\Omega \mathscr{D}^J_{M,K}(\theta_i) + (-)^{I+K}\chi_{-\Omega}\mathscr{D}^J_{M,-K}(\theta_i)\right\} \tag{20}$$

Here Ω labels the intrinsic state, and I, M, K are the angular momentum, its projection on the z-axis and on the symmetry axis, respectively.

The electric and magnetic multipole operators in the laboratory frame are written as the sum of single-particle and cluster contributions

$$\begin{aligned}\mathscr{M}_{el}(\lambda,\mu) &= T^{\lambda,s.p.}_{\mu,el} + T^{\lambda,c}_{\mu,el}\\ \mathscr{M}_{mag}(\lambda,\mu) &= T^{\lambda,s.p.}_{\mu,mag} + T^{\lambda,c}_{\mu,mag}\end{aligned} \tag{21}$$

The matrix elements of the operators in Eq. (21) can be calculated in the standard way by transforming them to the body-fixed frame

$$\mathscr{M}_{\lambda,\mu} = \sum_\nu \mathscr{D}^\lambda_{\mu\nu}(\theta_i)\mathscr{M}'_{\lambda,\nu} \tag{22}$$

and using

$$\int \mathscr{D}^{I'\dagger}_{M',K'}\mathscr{D}^\lambda_{\mu,\nu}\mathscr{D}^I_{M,K}d\varphi d\psi\sin\theta d\theta = \frac{8\pi}{2I'+1}\langle IM\lambda\mu|I'M'\rangle\langle IK\lambda\nu|I'K'\rangle. \tag{23}$$

The transition probabilities defined as

$$B(\lambda;\Omega',I',M',K'\to\Omega,I,M,K) = \sum_{\substack{M\\ \mu}}\left|\langle\Omega,IKM|\mathscr{M}_{\lambda,\mu}|\Omega',I'M'K'\rangle\right|^2, \tag{24}$$

where the sum is over the components μ and over the final component M, can be written as

$$B(\lambda;\Omega',I',M',K'\to\Omega,I,M,K)=\Big|\Big[\langle I',K';\lambda,K-K'|I,K\rangle\times \Big(\delta_{v,v'}G_\lambda(\Omega,\Omega')+\delta_{\Omega,\Omega'}G_{\lambda,c}\Big)+(-)^{I+K}\langle I',K';\lambda,-K-K'|I,-K\rangle \times\Big(\delta_{v,v'}\tilde{G}_\lambda(\Omega,-\Omega')+\delta_{\Omega,-\Omega'}G_{\lambda,c}\Big)\Big]\Big|^2. \tag{25}$$

The two terms in Eq. (25) come from the symmetrization of the wave function in Eq. (20), and

$$\begin{aligned} G^{(el,mag),s.p.}_{\lambda,K-K'} &= \int d^3\Omega' \mathscr{M}_{\lambda,K-K'}\chi_\Omega\chi^*_{\Omega'} \\ \tilde{G}^{(el,mag),s.p.}_{\lambda,-K-K'} &= \int d^3\Omega' \mathscr{M}_{\lambda,-K-K'}\chi_\Omega\chi^*_{-\Omega'}. \end{aligned} \tag{26}$$

We note that the second term in Eq. (25) contributes only in the case $\lambda \geq K+K'$.

Similarly, the electric multipole moments defined as

$$Q^{(\lambda)}(K,I)=\sqrt{\frac{16\pi}{2\lambda+1}}\langle\Omega,K,I,M=I|\mathscr{M}_{el}(\lambda,0)|\Omega,K,I,M=I\rangle \tag{27}$$

can be rewritten as

$$\begin{aligned} Q^{(\lambda)}(K,I)=&\sqrt{\frac{16\pi}{2\lambda+1}}\langle I,K,\lambda,0|I,K\rangle\langle I,I,\lambda,0|I,I\rangle\times \\ &\times\Big(G^{el,s.p.}_{\lambda,K-K'}(\Omega,\Omega)+G^{el,c}_{\lambda,K-K'}\Big) \end{aligned} \tag{28}$$

and the magnetic multipole moments defined as

$$\mu^{(\lambda)}(K,I)=\sqrt{\frac{4\pi}{2\lambda+1}}\langle\Omega,K,I,M=I|\mathscr{M}_{mag}(\lambda,0)|\Omega,K,I,M=I\rangle \tag{29}$$

can be written as

$$\begin{aligned} \mu^{(\lambda)}(K,I)=&\sqrt{\frac{4\pi}{2\lambda+1}}\langle I,K,\lambda,0|I,K\rangle\langle I,I,\lambda,0|I,I\rangle\times \\ &\times\Big(G^{mag,s.p.}_{\lambda,K-K'}(\Omega,\Omega)+G^{mag,c}_{\lambda,K-K'}\Big) \end{aligned} \tag{30}$$

To complete the calculation we need to specify the single particle and collective contributions. The single particle contribution is written in the standard form [58,59].

$$\begin{aligned} T^{el,s.p.}_{\lambda,\mu} &= e_{eff,cm}r^\lambda Y_{\lambda\mu}(\theta,\phi) \\ T^{mag,s.p.}_{\lambda,\mu} &= \frac{\hbar c}{2mc^2}\left(g_s\vec{s}+\frac{2}{\lambda+1}g_l\vec{l}\right)\cdot\nabla\left[r^\lambda Y_{\lambda\mu}(\theta,\phi)\right] \end{aligned} \tag{31}$$

where $e_{eff,cm}$ is the effective charge center-of-mass corrected [59]

$$e_{eff}=\begin{cases} e+(-)^\lambda\frac{Ze}{A^\lambda} & \text{for proton} \\ (-)^\lambda\frac{Ze}{A^\lambda} & \text{for neutron} \end{cases} \tag{32}$$

and

$$\begin{cases} g_s = 5.5855 & g_l = 1 \quad \text{for proton} \\ g_s = -3.8256 & g_l = 0 \quad \text{for neutron.} \end{cases} \tag{33}$$

The center-of-mass effective charges are $-Ze/A$ for $E1$ transitions and essentially zero for $\lambda > 1$. In the case of ^{9}Be, they are $-0.44e$ for $E1$, $0.049e$ for $E2$, and $0.005e$ for $E3$. The cluster contribution depends on the vibrational quantum number v of Eq. (12), and on the charge and magnetization distribution. The electric cluster contribution can be evaluated using the algebraic cluster model [44–46]. The electric cluster operator in the intrinsic frame has only the zeroth component $T^{el,c}_{\lambda,0}$ (axial symmetry). Its matrix elements are obtained from knowledge of the vibrational wave functions ψ_{vib}. For ground vibrational state to ground vibrational state they are given by

$$\int \psi_{v'=0}(T^{(\lambda)}_0)_c \psi_{v=0} d\tau = Z\beta^\lambda \sqrt{\frac{2\lambda+1}{4\pi}}, \tag{34}$$

where $\lambda = 0, 2, 4, \cdots =$ even, and $d\tau$ is the volume element. From this, we simply obtain

$$G^{el,c}_\lambda = Z\beta^\lambda \sqrt{\frac{2\lambda+1}{4\pi}}. \tag{35}$$

For odd multipoles, $\lambda = 1, 3, 5, \ldots$, the situation is more complicated since the single particle contribution essentially vanishes for $\lambda = 3, 5, \ldots$. In this case we need to introduce the coupling of the center of mass coordinate with the multipole moments $Q^{(\lambda)}$, $\lambda = 2, 4, \ldots$ of the cluster. This coupling introduces additional terms for $\lambda = 3, 5, \ldots$. We take for the electric transition operators of odd multipolarity the form

$$\begin{aligned} T^{(E1)} &= e^{(1)}_{eff} r Y_{1\mu}(\theta,\phi) \\ T^{(E3)} &= \left[e^{(3)}_{eff} r^3 + e^{(1)}_{eff} Z\beta^2 \sqrt{\frac{5}{4\pi}} r \right] Y_{3\mu}(\theta,\phi) \\ T^{(E5)} &= \left[e^{(5)}_{eff} r^5 + e^{(1)}_{eff} Z\beta^4 \sqrt{\frac{9}{4\pi}} r \right] Y_{5\mu}(\theta,\phi) \end{aligned} \tag{36}$$

where, from Eq. (32), for ^{9}Be, $e^{(1)}_{eff} = -\frac{4}{9}e$, $e^{(3)}_{eff} = -\frac{4}{729}e \approx 0$, $e^{(5)}_{eff} \approx 0$.

The magnetic cluster contribution is rather difficult to evaluate. It is proportional to the integral

$$\int \vec{\mathscr{R}}(\vec{r}) \cdot \vec{\nabla} \left(r^\lambda Y_{\lambda\mu}(\theta,\phi) \right) d^3\vec{r} \tag{37}$$

where $\vec{\mathscr{R}}(\vec{r})$ is the collective angular momentum density [39]. Since the cluster is composed of two spin-less α-particles, we take for simplicity

$$G^{mag,c}_\lambda = 0. \tag{38}$$

This choice is the same as that taken in Ref. [9] within the framework of the Nilsson model.

By expanding the wave function of the intrinsic states as in Eq. (11), and using the standard form of the matrix elements [58], we can then write the final expression for the electric

$$\begin{aligned} G^{el,s.p.}_{\lambda,-m'+m} = \sum_{\substack{nljm \\ n'l'j'm'}} & c_{nljm} c'_{n'l'j'm'} \langle n,l|r^\lambda|n',l'\rangle (-)^{-m'+m} \sqrt{\frac{(2j+1)(2\lambda+1)}{4\pi(2j'+1)}} \times \\ & \langle j,-m;\lambda,-m'+m|j',-m'\rangle \langle j,-\frac{1}{2};\lambda,0|j',-\frac{1}{2}\rangle \frac{1}{2}[1+(-)^{l+\lambda+l'}] \end{aligned} \tag{39}$$

and magnetic single-particle multipoles

$$G^{el,s.p.}_{\lambda,-m'+m} = \sum_{\substack{nljm \\ n'l'j'm'}} (-)^{j-m} c_{nljm} c'_{n'l'j'm'} \langle n,l|r^{\lambda-1}|n',l'\rangle \sqrt{\lambda(2j+1)(2j'+1)}$$
$$\frac{(2\lambda+1)}{\lambda+1} \begin{pmatrix} j & \lambda & j' \\ -m & -m'+m & m' \end{pmatrix} \Bigg[2g_l \sqrt{j'(j'+1)(2j'+1)}$$
$$(-)^{l+j+1/2} \begin{Bmatrix} j & \lambda & j' \\ 1 & j' & \lambda-1 \end{Bmatrix} \begin{Bmatrix} l & j & 1/2 \\ j' & l' & \lambda-1 \end{Bmatrix} + \left(\frac{\lambda+1}{2} g_s - g_l\right)$$
$$\sqrt{6} \begin{Bmatrix} l & 1/2 & j \\ l' & 1/2 & j' \\ \lambda-1 & 1 & \lambda \end{Bmatrix} \Bigg] \langle l||Y_{\lambda-1}||l'\rangle. \tag{40}$$

A computer program has been written by one of us (V. Della Rocca) to evaluate the matrix elements, Eqs. (39), and (40). By adding the cluster contribution, we can then evaluate the corresponding $B(E\lambda)$ values and moments $Q^{(\lambda)}$, $\mu^{(\lambda)}$.

3.4.1. Comparison with experiment

The formulas of the previous section allow a simple and direct comparison with experiment. Electric transitions within a rotational band are dominated by the cluster contribution. For the ground state $K^P = 3/2^-$ rotational band we have

$$B(E2; 3/2, I' \to 3/2, I) = \left(Ze\beta^2 \sqrt{\frac{5}{4\pi}}\right)^2 \langle I', 3/2, 2, 0|I, 3/2\rangle^2 \tag{41}$$

and quadrupole moment

$$Q^{(2)}(3/2, I) = \left(\sqrt{\frac{16\pi}{5}} Ze\beta^2 \sqrt{\frac{5}{4\pi}}\right) \langle I, 3/2, 2, 0|I, 3/2\rangle \langle I, I, 2, 0|I, I\rangle. \tag{42}$$

Inserting the value of $\beta = 1.82$ fm we obtain the results of Table 14. The agreement between the parameter free theory (β has been determined from the moment of inertia of ^{8}Be) and experiment is excellent and provides the strongest argument for the cluster structure of ^{9}Be as ^{8}Be+n.

Magnetic transitions within a rotational band are determined by the single-particle contribution. For the ground state $K^P = 3/2^-$ rotational band we have

$$B(M1; 3/2, I' \to 3/2, I) = \langle I', 3/2, 1, 0|I, 3/2\rangle^2 |G_1(3/2)|^2 \tag{43}$$

and magnetic moments

$$\mu^{(1)}(3/2, I) = \sqrt{\frac{4\pi}{3}} \langle I, 3/2, 1, 0|I, 3/2\rangle \langle I, I, 1, 0|I, I\rangle G_1(3/2). \tag{44}$$

Inserting $g_s = -3.82$ we have results of Table 14. The magnetic moment appears to be well reproduced while $B(M1)$ is a factor of 2 smaller.

In addition to in-band transitions, out-of band $E1$ transitions between $K^P = 3/2^-$ and $K^P = 1/2^+$ intrinsic states have been measured. From Eq. (32), the $E1$ effective charge is here $e_{eff}(E1) = -\frac{4}{9}e$. With this value we obtain the results of Table 14. The agreement between the calculation and experiment for the $B(E1; 3/2^- \to 1/2^+)$ is good, but not so for

Table 14
Comparison between NDT [50] and cluster-shell model, CSM. Quadrupole moment of the ground state $3/2^-$ in efm^2 and $B(E2)$ values in e^{2}fm^4. Magnetic moment of the ground state $3/2^-$ in μ_N and $B(M1)$ values in μ_N^2. $B(E1)$ values in e^2 fm^2.

	NDT	CSM
$Q(3/2^-)$	5.288(38)	5.30
$B(E2; 3/2^- \to 5/2^-)$	40.5(30)	35.9
$B(E2; 3/2^- \to 7/2^-)$	18(8)	20.0
$\mu(3/2^-)$	$-1.1778(9)$	-1.13
$B(M1; 3/2^- \to 5/2^-)$	0.82(3)	0.35
$B(E1; 3/2^- \to 1/2^+)$	0.029(3)	0.024
$B(E1; 3/2^- \to 5/2^+)$	0.015(12)	0.0048

$B(E1; 3/2^- \to 5/2^+)$. However, the experimental error in the latter is large (80%) and the calculated value is within experimental error.

In addition to $E2$, $M1$ and $E1$ transitions, higher multipoles have been extracted from electron scattering experiments [60]. Although some model dependence is implied in this extraction and therefore the values differ somewhat from those reported above, nonetheless it is of interest to compare these values with the calculations. This is done in Table 15, which represents a summary of all results. Note that in this table the magnetic transitions are in units of e^{2}fm$^{2\lambda}$, as it is usual in electron scattering [60], and not in units of $\mu_N$fm$^{2\lambda-2}$, as in the nuclear data tables [50]. We see again from this table that while the collective $E2$ transitions are very well described by the cluster model, and the single particle transitions $M1$ and $E1$ are reasonably well described by the calculation, all the other transitions $M2$, $M3$, $M4$ and $E3$, $E5$ are, at best, qualitatively described and in some cases poorly described. This may be due, in part, to the way in which $B(E\lambda)$ and $B(M\lambda)$ values have been extracted from experiment, by taking the limit $q \to 0$ of high-momentum transfer form factor data. The experimental data for higher multipoles are in disagreement also with the large scale shell model calculation reported in Ref. [60] as one can see from the same Table 15. The shell model calculation, however, contains effective charges which are adjusted for each multipolarity, $E2$, $E1$, $E3$, $E5$. The cluster calculation instead does not contain any effective charge, apart from the CM E1.

3.5. Comparison with ab initio calculations

$E2$ and $M1$ transitions and moments have been calculated within the framework of both the GFMC method [34] and the no-core shell model (NCCI) [38]. We consider here only the quadrupole moment and the magnetic moment, Table 16, and compare them with GFMC. Values for NCCI are not explicitly reported in [38] and we will therefore not consider them here. The agreement between GFMC and experiment is excellent. In NCCI, also $B(E2)$ values along the rotational band built on $K^P = 3/2^-$ and $K^P = 1/2^-$ states have been calculated as shown in Fig. 14 of Ref. [38]. They clearly show the occurrence of rotational bands as in the cluster model, although one to one comparison with the cluster model would require an extraction of the numerical values from the figure which is beyond the scope of this paper. Ab initio calculations of the other multipoles, $E1$, $M2$, ..., are not available.

Table 15
$Q(3/2^-)$ in efm^2 and $\mu(3/2^-)$ in μ_N; $B(E\lambda)$ and $B(M\lambda)$ values in e^2 fm$^{2\lambda}$. Note the unusual units of $B(M\lambda)$. NDT from [50] and (e, e') from [60]. When no experimental data are available for a particular transition, we still show the values obtained using the cluster shell-model (CSM) for comparison with the shell-model (SM).

	NDT	(e, e')	SM	CSM
$Q(3/2^-)$	5.288(38)	5.86(6)	4.35	5.30
$\mu(3/2^-)$	−1.1778(9)	−1.16(2)	−1.27	−1.13
$B(E2; 3/2^- \to 3/2^-_1)$	–	17.1(3)	9.43	14.0
$B(E2; 3/2^- \to 5/2^-_1)$	40.5(30)	46.0(5)	32.2	35.9
$B(E2; 3/2^- \to 7/2^-_1)$	18(8)	33(1)	12.7	20.0
$B(E1; 3/2^- \to 1/2^+_1)$	0.029(3)	0.034(3)	0.0045	0.024
$B(E1; 3/2^- \to 5/2^+_1)$	0.015(12)	0.029(5)	0.0039	0.0048
$B(E1; 3/2^- \to 3/2^+_1)$	–	–	0.0006	0.019
$B(E3; 3/2^- \to 5/2^+_1)$	–	0.9(6)	12.5	0.24
$B(E3; 3/2^- \to 3/2^+_1)$	–	–	3.41	0.014
$B(E3; 3/2^- \to 9/2^+_1)$	–	216(5)	17.6	0.59
$B(E3; 3/2^- \to 7/2^+_1)$	–	57(6)	26.5	0.40
$B(E5; 3/2^- \to 9/2^+_1)$	–	–	–	1.36
$B(E5; 3/2^- \to 7/2^+_1)$	–	–	–	0.03
$B(M1; 3/2^- \to 3/2^-_1)$	–	0.0059(1)	–	0.0056
$B(M1; 3/2^- \to 5/2^-_1)$	0.0089(9)	0.0090(3)	0.0068	0.0038
$B(M3; 3/2^- \to 3/2^-_1)$	–	4.4(3)	9.72	23.9
$B(M3; 3/2^- \to 5/2^-_1)$	–	0.5(3)	2.22	9.99
$B(M2; 3/2^- \to 1/2^+_1)$	–	0.023(8)	0.022	0.094
$B(M2; 3/2^- \to 5/2^+_1)$	–	0.16(2)	0.018	0.038
$B(M2; 3/2^- \to 3/2^+_1)$	–	–	0.013	0.10
$B(M4; 3/2^- \to 5/2^+_1)$	–	58(3)	127.6	243.9
$B(M4; 3/2^- \to 9/2^+_1)$	–	174(16)	223.8	404.8
$B(M4; 3/2^- \to 7/2^+_1)$	–	–	35.9	36.1

Table 16
Comparison between NDT [50], CSM, and GFMC results.

	NDT	CSM	GFMC
$Q(3/2^-)$	5.288(38)	5.30	5.1(1)
$\mu(3/2^-)$	−1.1778(9)	−1.13	−1.18(1)

3.5.1. Comparison with LCAO and 3-body calculations

$B(E2)$, quadrupole moments Q, $B(M1)$, and magnetic moments have been calculated within the framework of LCAO and 3-body cluster. Since the values in [6,7] are given only in figures and thus difficult to extract and also depend crucially on the details of the interactions, Set I and II, we compare in Table 17 only with results from 3-body calculations [22], Table III. We see here a remarkable agreement between 3-body [22] and CSM calculations.

Table 17
Comparison between 3-body calculations [22] and CSM. Q in efm^2, μ in μ_N, $B(EL)$ in e^{2}fm^{2L}, and $B(M1)$ in μ_N^2. The values given in [22] in W.u. have been converted to appropriate values e^{2}fm^{2L}. Two values of $B(E1)$ are given in [22], both included here.

	NDT	3-BODY [22]	CSM
$Q(3/2^-)$	5.288(38)	5.13	5.30
$\mu(3/2^-)$	−1.1778(9)	−1.169	−1.13
$B(E2; 3/2^- \to 5/2^-)$	40.5(30)	36.7	35.9
$B(M1; 3/2^- \to 5/2^-)$	0.82(3)	0.34	0.35
$B(E1; 3/2^- \to 1/2^+)$	0.029(3)	0.046/0.034	0.024

3.6. Form factors in electron scattering

Form factors in electron scattering are again split into a single-particle and collective cluster contribution

$$F(q; I, K \to I', K') = F^{s.p.}(q; I, K \to I', K') + F^{c}(q; I, K \to I', K') \tag{45}$$

We assume that the collective contribution applies only to the longitudinal electric form factors. For even multipoles $\lambda = 0, 2, 4, \ldots$ it has the form of Eq. (10)

$$F_\lambda^{el,c}(q; I, K \to I', K') = \delta_{KK'} Z \sqrt{\frac{2\lambda+1}{4\pi}} \langle I, K, \lambda, 0 | I', K' \rangle e^{-\frac{q^2}{4\alpha}} j_\lambda(q\beta). \tag{46}$$

For odd multipoles $\lambda = 1, 3, 5, \ldots$ we take, for the radial dependence

$$\begin{aligned}
\lambda = 1 \qquad & e_{eff}^{(1)} j_1(qr) + e_{eff}^{(1)} Z \sqrt{\frac{5}{4\pi}} e^{-\frac{q^2}{4\alpha}} j_2(q\beta) j_1(qr) \\
\lambda = 3 \qquad & e_{eff}^{(3)} j_3(qr) + e_{eff}^{(1)} \Big[Z \sqrt{\frac{5}{4\pi}} e^{-\frac{q^2}{4\alpha}} j_2(q\beta) j_1(qr) + \\
& \qquad + Z \sqrt{\frac{9}{4\pi}} e^{-\frac{q^2}{4\alpha}} j_4(q\beta) j_1(qr) \Big] \\
\lambda = 5 \qquad & e_{eff}^{(5)} j_5(qr) + e_{eff}^{(1)} \Big[Z \sqrt{\frac{9}{4\pi}} e^{-\frac{q^2}{4\alpha}} j_4(q\beta) j_1(qr) + \\
& \qquad + Z \sqrt{\frac{13}{4\pi}} e^{-\frac{q^2}{4\alpha}} j_6(q\beta) j_1(qr) \Big]
\end{aligned} \tag{47}$$

where, from Eq. (32) we have for ^{9}Be, $e_{eff}^{(1)} = -\frac{4}{9}$e,$e_{eff}^{(3)} \approx 0$, and $e_{eff}^{(5)} \approx 0$.

The single-particle contribution instead gives rise to longitudinal electric, transverse magnetic and transverse electric form factors. These contributions were derived in the laboratory frame by De Forest and Walecka [61] but need to be converted to the intrinsic frame for use in the cluster shell model. In the following subsections, we give, for future reference, the explicit formulas, and note that a computer program has been written to evaluate these contributions.

From the form factors, one can also evaluate the $B(E\lambda)$ values as

$$B(\lambda; I, K \to I', K') = [(2\lambda+1)!!]^2 \lim_{q \to 0} \left| \frac{F_\lambda(q)}{q^\lambda} \right|. \tag{48}$$

3.6.1. Longitudinal electric form factors

The single particle contributions to the longitudinal electric form factor, also called Coulomb form factor, CL, in [61] can be written as

$$F_\lambda^{el,long}(q; I, K \to I', K') = \langle I, K, \lambda, K' - K | I', K' \rangle C_\lambda^{el,long}(q) + \\ + (-)^{I'+K'} \langle I, K, \lambda, -K' - K | I', -K' \rangle \tilde{C}_\lambda^{el,long}(q) \tag{49}$$

The longitudinal electric coefficient, $C_\lambda^{el,long}(q)$, for multipolarity $\lambda = L$ is given by

$$C_\lambda^{el,long}(q) = \sum_{\substack{nljm \\ n'l'j'm'}} c_{nljm} c_{n'l'j'm'} \langle n, l | j_\lambda(qr) | n', l' \rangle \sqrt{\frac{(2j+1)(2\lambda+1)}{4\pi(2j'+1)}} \\ (-)^{-m'+m} \langle j, -m; \lambda, -m'+m | j', -m' \rangle \langle j, -\frac{1}{2}; \lambda, 0 | j', -\frac{1}{2} \rangle \frac{1}{2} [1 + (-)^{l+\lambda+l'}] \tag{50}$$

A similar expression holds for $\tilde{C}_\lambda^{el}(q)$, which however contributes only in the unlikely case of $\lambda \geq K + K'$.

3.6.2. Transverse magnetic form factors

We write the transverse magnetic form factors as

$$F_\lambda^{mag,trans}(q; I, K \to I', K') = \langle I, K, \lambda, K' - K | I', K' \rangle C_\lambda^{mag,trans}(q) \\ + (-)^{I'+K'} \langle I, K, \lambda, -K' - K | I', -K' \rangle \tilde{C}_\lambda^{mag,trans}(q) \tag{51}$$

The coefficient $C_\lambda^{mag,trans}(q)$ has a complicate expression involving the magnetic moment of the odd-particle, $\mu = 2.79$ or -1.91 for proton or neutron respectively, its charge $e = 1$ or 0, and the nucleon mass m_N. Introducing the notation of [61]

$$M_J^M(\vec{r}) = j_J(qr) Y_{JM}(\theta, \phi) \\ \mathbf{M}_{JL}^M(\vec{r}) = j_L(qr) \mathbf{Y}_{JL1}^M(\theta, \phi) \tag{52}$$

we have

$$C_\lambda^{mag,trans}(q) = \sum_{\substack{nljm \\ n'l'j'm'}} c_{nljm} c_{n'l'j'm'} \frac{iq}{m_p} \times \\ \Big\{ -\frac{\mu_i}{q} \sqrt{\frac{\lambda}{2\lambda+1}} \langle n, \frac{1}{2}, l, j, m | \mathbf{M}_{\lambda,\lambda+1}^{-m'+m} \cdot \boldsymbol{\sigma} | n', \frac{1}{2} l', j', m' \rangle \\ + \frac{\mu_i}{q} \sqrt{\frac{\lambda+1}{2\lambda+1}} \langle n, \frac{1}{2} l, j, m | \mathbf{M}_{\lambda,\lambda-1}^{-m'+m} \cdot \boldsymbol{\sigma} | n', \frac{1}{2}, l', j', m' \rangle \\ - \frac{e_i}{2} \langle n, \frac{1}{2}, l, j, m | \mathbf{M}_{\lambda,\lambda}^{-m'+m} \cdot \nabla | n', \frac{1}{2}, l', j', m' \rangle \Big\}, \tag{53}$$

where i denotes proton or neutron. A similar expression holds for $\tilde{C}_\lambda^{mag,trans}$.

For ^{9}Be only the terms proportional to μ survive, and the coefficient $C_\lambda^{mag,trans}(q)$ have the explicit expression

$$C_\lambda^{mag,trans}(q) = \sum_{\substack{nljm \\ n'l'j'm'}} c_{nljm} c_{n'l'j'm'} q \frac{\mu_i}{2} \sqrt{6} \begin{pmatrix} j & \lambda & j' \\ -m & -m'+m & m' \end{pmatrix} (-1)^{l+j-m}$$
$$\sqrt{\frac{(2l'+1)(2l+1)(2j'+1)(2j+1)(2\lambda+1)}{4\pi}} \Big\{ -\sqrt{\frac{\lambda}{2\lambda+1}} \sqrt{2(\lambda+1)+1}$$
$$\begin{Bmatrix} l & l' & \lambda+1 \\ 1/2 & 1/2 & 1 \\ j & j' & \lambda \end{Bmatrix} \begin{pmatrix} l & \lambda+1 & l' \\ 0 & 0 & 0 \end{pmatrix} \langle n, l | j_{\lambda+1}(qr) | n', l' \rangle \tag{54}$$
$$+ \sqrt{\frac{\lambda+1}{2\lambda+1}} \sqrt{2(\lambda-1)+1} \begin{Bmatrix} l & l' & \lambda-1 \\ 1/2 & 1/2 & 1 \\ j & j' & \lambda \end{Bmatrix} \begin{pmatrix} l & \lambda-1 & l' \\ 0 & 0 & 0 \end{pmatrix}$$
$$\langle n, l | j_{\lambda-1}(qr) | n', l' \rangle \Big\}.$$

3.6.3. Transverse electric form factors

We write this form factor as

$$F_\lambda^{el,trans}(q; I, K \to I', K') = \langle I, K, \lambda, K'-K | I', K' \rangle C_\lambda^{el,trans}(q) + (-)^{I'+K'} \langle I, K, \lambda, -K'-K | I', -K' \rangle \tilde{C}_\lambda^{el,trans}(q) \tag{55}$$

Introducing the notation of eq. (51), we have

$$C_\lambda^{el,trans}(q) = \sum_{\substack{nljm \\ n'l'j'm'}} c_{nljm} c_{n'l'j'm'} \frac{1}{m_p} q \times$$
$$\Big\{ -\frac{e_i}{q} \sqrt{\frac{\lambda}{2\lambda+1}} \langle n, \frac{1}{2}, l, j, m | \mathbf{M}_{\lambda,\lambda+1}^{-m'+m} \cdot \nabla | n', \frac{1}{2} l', j', m' \rangle \tag{56}$$
$$+ \frac{e_i}{q} \sqrt{\frac{\lambda+1}{2\lambda+1}} \langle n, \frac{1}{2} l, j, m | \mathbf{M}_{\lambda,\lambda-1}^{-m'+m} \cdot \nabla | n', \frac{1}{2}, l', j', m' \rangle$$
$$+ \frac{\mu_i}{2} \langle n, \frac{1}{2}, l, j, m | \mathbf{M}_{\lambda,\lambda}^{-m'+m} \cdot \boldsymbol{\sigma} | n', \frac{1}{2}, l', j', m' \rangle \Big\}$$

and similarly for $\tilde{C}_\lambda^{el,trans}(q)$. For ^{9}Be only the term proportional to μ survives.

3.6.4. Comparison with experiment

Form factors in electron scattering were extensively investigated in the 1970s [62–65]. A comprehensive experiment was done at the MIT-Bates Linear Accelerator in 1991 [60]. In this section, we compare our calculated form factors with those from [60]. In this reference, the authors plot the form factors

$$|F_\lambda(q)|^2 = \frac{\sqrt{4\pi}}{Z} |F_\lambda(q; \uparrow)|^2 \tag{57}$$

for longitudinal (Coulomb), transverse magnetic and transverse electric.

The longitudinal form factors for transitions within the ground state $K^P = 3/2^-$ rotational band are determined by the cluster contribution. We find that these form factors are described almost perfectly by the calculation, as shown in Fig. 9 top. This is a remarkable result since there

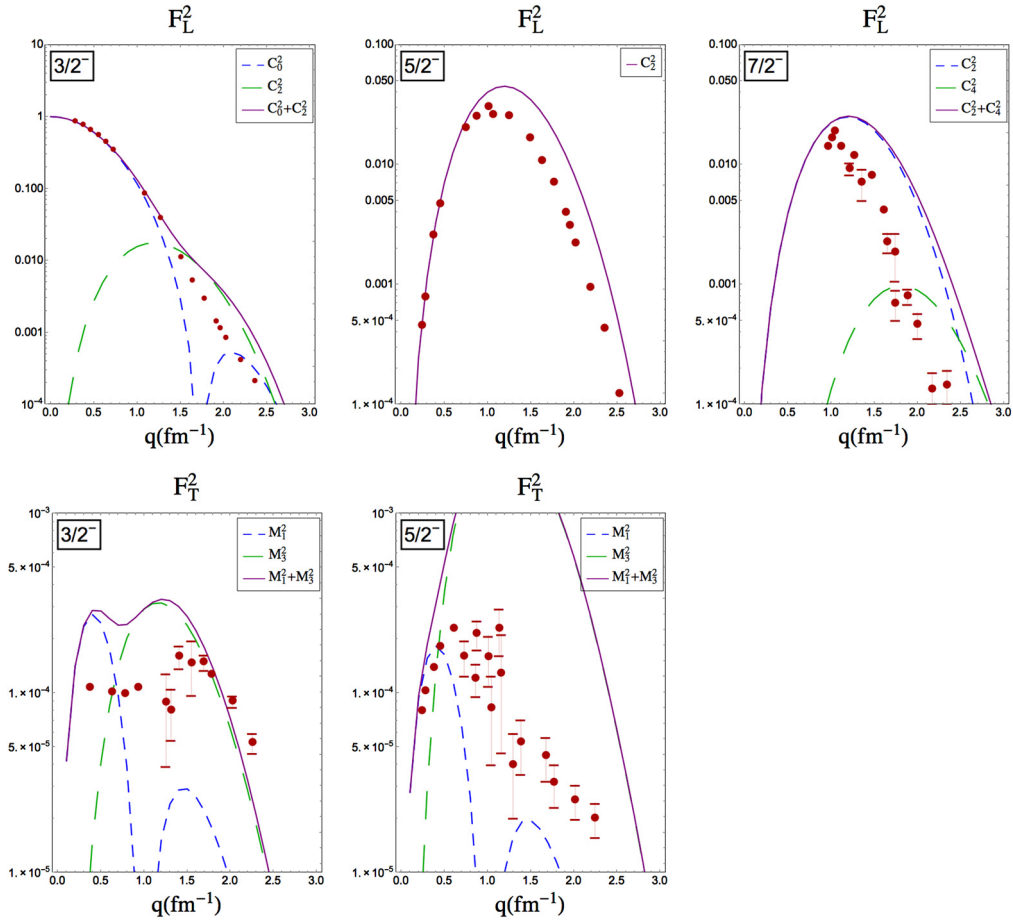

Fig. 9. Comparison between calculated and experimental form factors for members of the ground state $K^P = 3/2^-$ rotational band. Top panels: Longitudinal form factors. Bottom panels: Transverse magnetic form factors.

are no free parameters in the calculation, the value of β having been fixed by the spectrum of ^{8}Be. In contrast, shell model calculations require large $E2$ effective charges [60].

Transverse magnetic form factors for transitions within the ground state band $K^P = 3/2^-$ are instead determined by single particle contributions. In Fig. 9 bottom we show a comparison between experimental and calculated form factors for transverse multipoles. The agreement here is not good, especially for the ground state $3/2^-$, in spite of the fact that we calculated correctly the magnetic moment, Table 14. In particular the calculated $M3$ is much larger than experiment as in the corresponding $B(M3)$ in Table 14. In is not clear whether this disagreement is due to an experimental or a theoretical problem. The SM calculations also have the same problem.

The form factors for transitions between the ground state $K^P = 3/2^-$ and members of the rotational band with $K^P = 1/2^+$ are obtained using the radial dependence in Eq. (47). A comparison between experimental and calculated form factors for transitions to the states $1/2^+$, $5/2^+$,

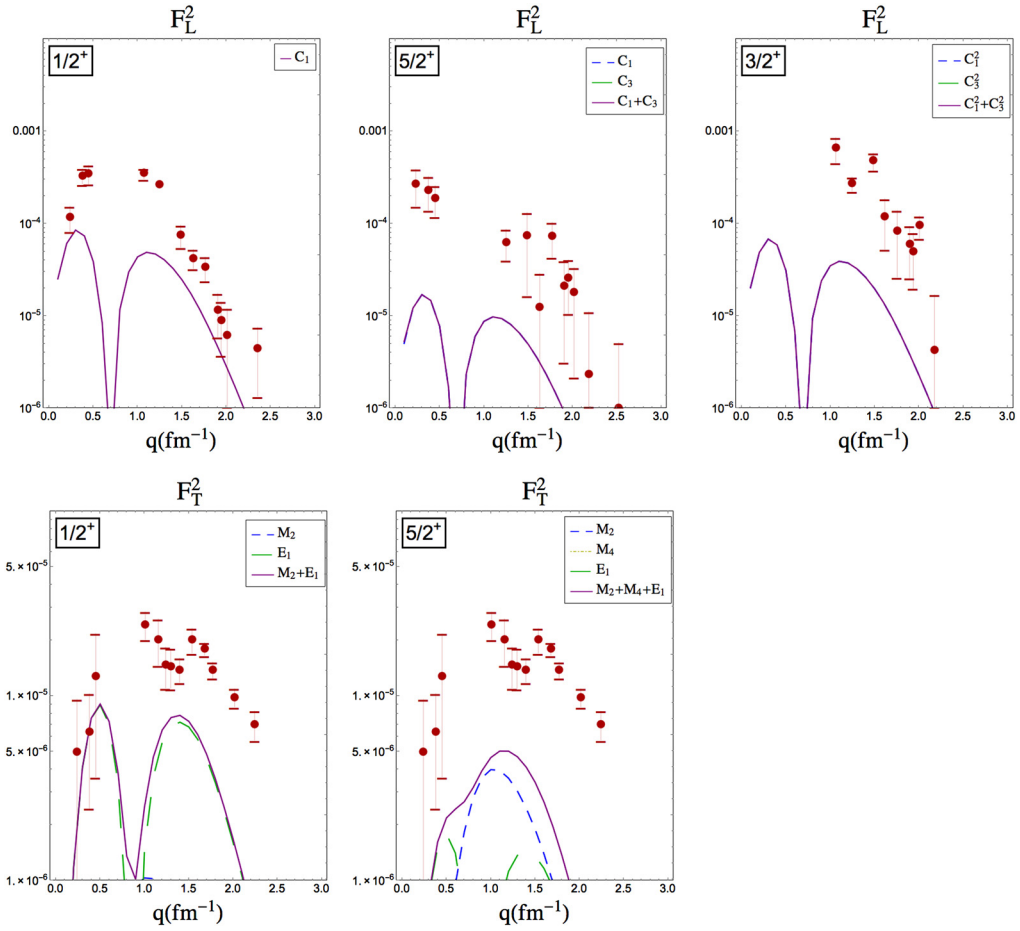

Fig. 10. Comparison between calculated and experimental form factors for members of the $K^P = 1/2^+$ rotational band. Top panels: Longitudinal form factors. Bottom panels: Transverse form factors.

$3/2^+$ is shown in Fig. 10 (top). It appears that the shapes of the $C1$ form factors are well described by the calculation but that the magnitude as obtained from the center-of-mass correction, Eq. (32), is too small. This requires the use of a larger value of $e^{(1)}_{eff}$, i.e. a rescaling of the results, as in Fig. 11.

3.6.5. Comparison with ab initio calculations

No calculation of form factor is available from ab initio calculations.

3.6.6. Comparison with LCAO and 3-body cluster

Form factors for the ground state band, $K^P = 3/2^-$, have been also calculated in LCAO and reported in Figs. 11 and 12 of [6] and in 3-body cluster and reported in Figs. 4 and 5 of [22]. Although it is not possible to make a direct comparison since the values are presented in figures, one can see that while the longitudinal form factors all are in good agreement with each other

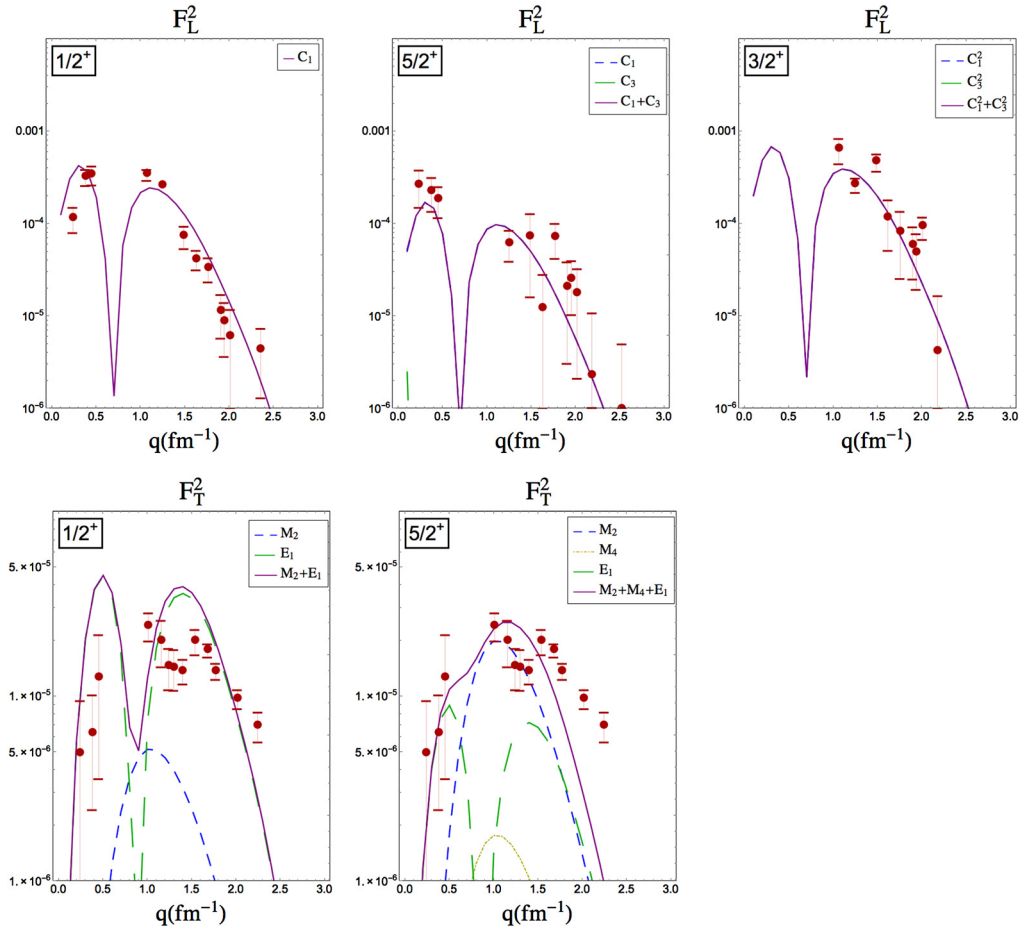

Fig. 11. Comparison between calculated scaled form factors and experimental form factors for members of the $K^P = 1/2^+$ rotational band. Top panels: Longitudinal form factors scaled by a factor of 10. Bottom panels: Transverse form factors scaled by a factor of 5.

and with data, the transverse form factors are not. The shapes of our transverse form factors $M1$ and $M3$ are in good agreement with Fig. 5 of [22], but their magnitude is not. In order to bring our transverse form factors in agreement with experiment we need a quenching factor of ≈ 0.7 in agreement with shell model and other calculations. This quenching comes from non-nucleonic degrees of freedom and two-body currents. We do not understand why the 3-body calculations do not need a quenching.

Form factors to the $1/2^+$ state were calculated in LCAO and reported in Fig. 10 of [7]. The LCAO methods gives a result similar to our Fig. 10, but much lower than experiment. Much elaborate calculations bring it in fair agreement with experiment. In contrast, a simple rescaling of our results gives perfect agreement with experiment, both for longitudinal and transverse form factors $3/2^- \rightarrow 1/2^+$. No form factors for $3/2^- \rightarrow 1/2^+$ transitions are reported in [22] and [24].

Table 18
Comparison between calculated and experimental [66] GT strength.

J^P	$E_x^{(p,n)}$	$B(GT)^{(p,n)}$	$E_x^{(^3He,t)}$	$B(GT)^{(^3He,t)}$	$B(GT)^{calc}$
$3/2^-$	0	0.91(15)	0.0(3)	0.66(18)	0.95
$5/2^-$	2.36	0.24(1)	2.358(7)	0.241(8)	0.63
$1/2^-$	2.71	0.33(4)	2.73(7)	0.718(24)	0.59
	2.79	1.13(5)			
$(5/2^-)$	4.3	0.28(1)	3.93(10)	0.360(12)	0.12

4. Beta transitions

The transition probability for β-decay can be calculated in a way similar to the calculation of the electromagnetic transition probability and is given thus by the quantities

$$D_{\substack{F,\\GT}}(n, K'I' \to KI) = \sum_{\mu,M} |\langle \Omega, I, K, L|\mathscr{D}_{F,GT}(\mu, M)|\Omega', I', K', M'\rangle|^2, \tag{58}$$

where F, GT denote Fermi and Gamow–Teller transitions, respectively, and n is the degree of forbiddenness. For $n = 0$, the transition operator is $\mathscr{D}_F = \tau_\pm$, $\mathscr{D}_{GT} = \tau_\pm \vec{\sigma}$. Beta-decay rates are usually quoted in terms of log ft values. For allowed transitions, $n = 0$, the ft values can be written as

Текст

$$ft = \frac{\mathscr{K}}{g_V^2 D(F)^2 + g_A^2 D(GT)^2} \tag{59}$$

where $\mathscr{K} = 2\pi^3\hbar^7 \ln 2/m^5c^4$, $g_V = 1$, $g_A = 1.269$ are the vector and axial vector coupling constants, and, using appropriate units, [59], $\mathscr{K} = 6163$ sec. Fermi transitions can occur only to states with the same K and I. Introducing a notation similar to that of Sect. 3, we have

$$D_F(K', I' \to K, I) = \delta_{KK'}\delta_{II'} \tag{60}$$

where K', I' are the quantum number of states in the decaying nucleus and K, I in the final nucleus. For Gamow–Teller transitions, one can use the analogy between the Gamow–Teller operator and the $M1$ operator of Sect. 3, obtaining

$$D_{GT}(K', I' \to K, I) = |\langle I', K', 1, K - K'|I, K\rangle \gamma_1|^2 \tag{61}$$

where

$$\gamma_1 = G_{M1}(g_s = 2g_A, g_l = 0), \tag{62}$$

and G_{M1} is given by Eq. (40). Assuming charge independence of the wave function, D_{GT} can be simply calculated using the wave functions obtained previously. A more elaborate calculation can be done by making use of the wave functions of ^{9}B to be discussed in the following section.

No data are available for the beta decay of ^{9}B into ^{9}Be, since the ground state of ^{9}B decays strongly to $2\alpha + p$. However, recently GT matrix elements have been measured [66] by means of $(^3He, t)$ and (p, n) reactions. The $B(GT)$ values are defined, in our notation, as

$$B(GT) = \frac{4\pi}{3} g_A^2 D_{GT}. \tag{63}$$

In Table 18, we show a comparison between our calculated values and experiment.

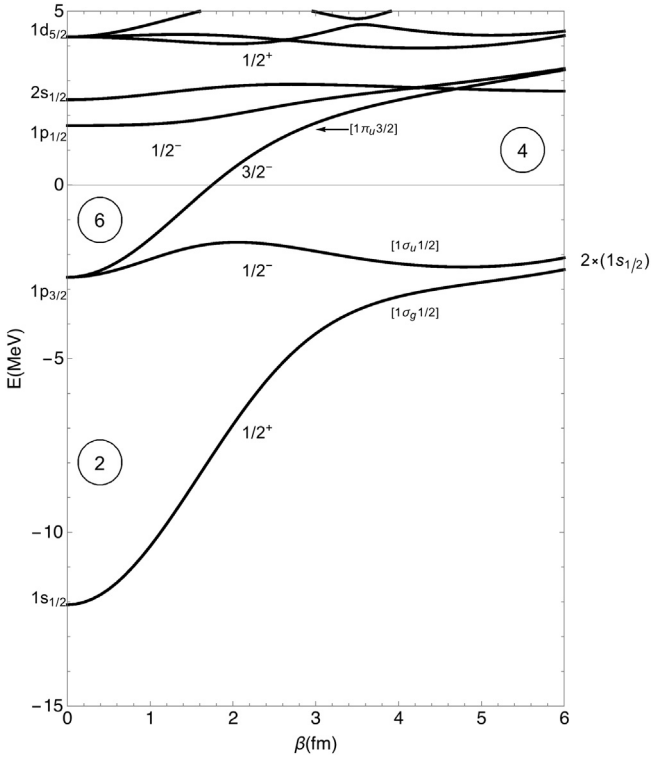

Fig. 12. Energy levels of a spin 1/2 proton in a Z_2 symmetric potential, with $V_0 = 20$ MeV, $\alpha = 0.1115$ fm^{-2}, $V_{0,C} = 2.43$ MeV, and $\alpha_C = 0.06$ fm^{-2}.

5. Structure of ^{9}B

We assume for ^{9}B a structure similar to ^{9}Be, with the odd neutron replaced by an odd-proton. The single particle levels, ϵ_Ω, and wave functions, χ_Ω, are obtained as in Sect. 3 but with the Coulomb interaction included [1]. The expression of the Coulomb interaction was given in Eq. (32) of [1]. For simplicity in the numerical solution of the eigenvalue problem for

$$H = \frac{\vec{p}^2}{2m} + V(\vec{r}) + V_{so}(\vec{r}) + V_C(\vec{r}), \tag{64}$$

we approximate $V_C(\vec{r})$ with a form similar to $V(\vec{r})$,

$$V_C(\vec{r}) = V_{0,C} \sum_{\lambda\mu} e^{-\alpha_C(r^2+\beta^2)} 4\pi i_\lambda(2\alpha_C\beta r) Y_{\lambda\mu}(\theta,\phi) \sum_{i=1}^{2} Y^*_{\lambda\mu}(\theta_i,\phi_i), \tag{65}$$

but with a different value of $\alpha = \alpha_C$. For ^{9}B, $V_{0c} = 2.43$ MeV and $\alpha_c = 0.06$ fm^{-2}. We have verified that our approximation is good within a few percent in the range $0 \le \beta \le 8$ fm. The single particle levels with the Coulomb interaction included are given in Fig. 12. We see here that at $\beta = 1.82$ fm all states $K^P = 3/2^-, 1/2^-, 1/2^+$ are unbound, in agreement with experiment. This is a remarkable result since there are no parameters in the calculation, the value of β having been determined from ^{8}Be.

Table 19
Comparison of intrinsic energies and Coulomb displacements with experiment. All units in MeV. The experimental error in ΔE_K is estimated from the width of the states in ^{9}Be and ^{9}B.

K^P	ϵ_K (calc)		$\Delta\epsilon_K$ (calc)	E_K (calc)		E_K (exp)		ΔE_K (exp)
	^{9}Be	^{9}B	$= \Delta E_K$ (calc)	^{9}Be	^{9}B	^{9}Be	^{9}B	
$3/2^-$	−1.78	0.14	1.92	−1.12	0.79	−1.66	0.18	1.84(2)
$1/2^-$	0.32	1.96	1.64	0.21	1.85	1.12	2.93	1.81(36)
$1/2^+$	1.35	2.81	1.46	0.98	2.48	0.02	1.78	1.76(52)

Table 20
The three components of the moment of inertia, $\mathscr{I}^2/m$, due to the odd proton and of the total moment of inertia $\mathscr{I}/m$. All values in fm^2.

K^P	$3/2^-$	$1/2^-$	$1/2^+$
$\mathscr{I}_x^n/m$	6.7	9.2	12.9
$\mathscr{I}_y^n/m$	6.7	9.2	12.9
$\mathscr{I}_z^n/m$	8.8	8.6	12.1
$\mathscr{I}_x/m$	47.5	50	53.7
$\mathscr{I}_y/m$	47.5	50	53.7
$\mathscr{I}_z/m$	23.1	22.9	26.4

In Table 19, we show a comparison between the single-particle intrinsic energies ϵ_K and the energies E_K of Eq. (12) in ^{9}Be and ^{9}B. From these we obtain the Coulomb energy displacements $\Delta\epsilon_K = \epsilon_K(^9B) - \epsilon_K(^9Be) = \Delta E_K$ and compare those with experiment. The value of ΔE_K for the ground state $3/2^-$ is in excellent agreement with data.

Repeating the calculations of Sect. 3, we calculate the moments of inertia, given in Table 20. These are slightly different from those in Table 6. The decoupling parameters are also slightly different,

$$\begin{aligned} a(1/2^-) &= 0.77 \\ a(1/2^+) &= 1.35 \end{aligned} \tag{66}$$

From the moment of inertia and the decoupling parameter we calculate the spectrum and compare it with experiment in Figs. 13 and 14.

Although no experimental data are available due to the fact that ^{9}B is unstable, we have calculated nonetheless the values of G_λ^{el}, $\tilde{G}_\lambda^{el}$ and G_λ^{mag}, $\tilde{G}_\lambda^{mag}$, which are needed for the evaluation of $B(E\lambda)$, $B(M\lambda)$ values and $Q^{(\lambda)}$ and $\mu^{(\lambda)}$ values in ^{9}B. These values, as well as details of all calculations reported here, are contained in Ref. [67] and can be obtained from us upon request.

The structure of ^{9}B was also calculated in the microscopic 3-body cluster model [22]. In Table 21 we compare the Coulomb displacements calculated in that model with our results. The CSM results are in excellent agreement with the 3-body results and with experiment for $K^P = 3/2^-$ but both deviate from experiment for $K^P = 1/2^-$ and $K^P = 1/2^+$.

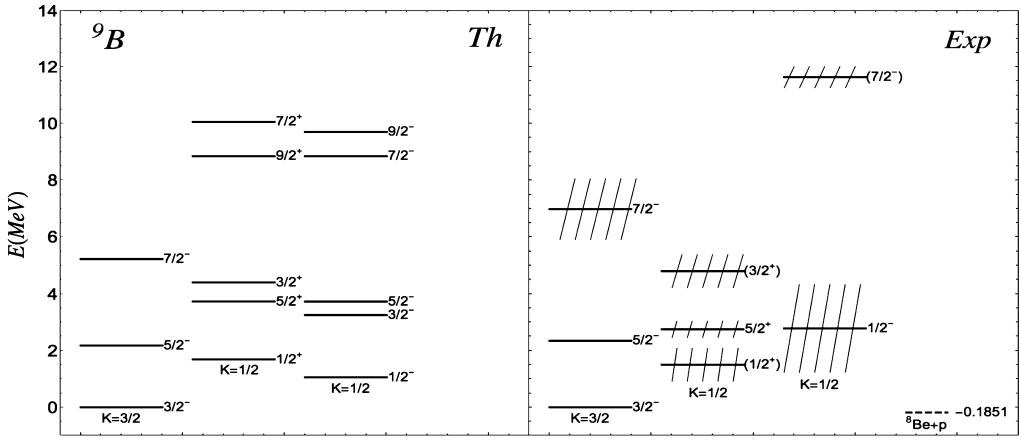

Fig. 13. Comparison between the energy levels of ^{9}B as predicted by the CSM and as obtained in experiment [50]. The observed level at 1.5 MeV is tentatively assigned to $1/2^+$ and that at 4.8 MeV to $3/2^+$ by analogy to ^{9}Be.

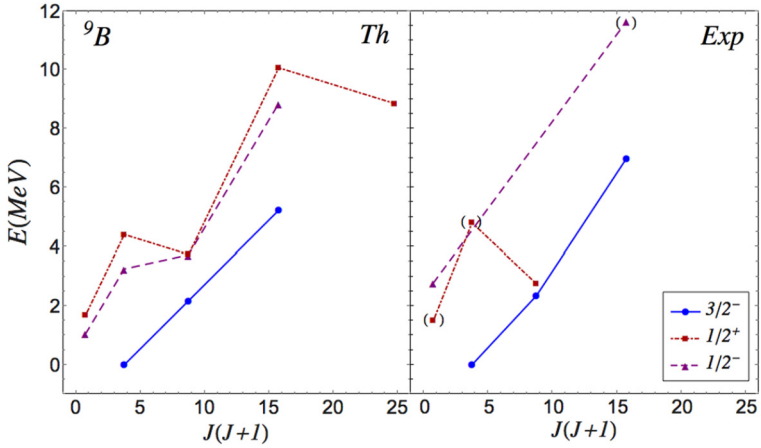

Fig. 14. Observed rotational bands in ^{9}B.

Table 21
Comparison of Coulomb displacements. All values in MeV. The experimental error in ΔE_K is estimated from the width of the states in ^{9}Be and ^{9}B.

K^P	ΔE_K (MeV)		
	CSM	3-BODY [22]	Exp
$3/2^-$	1.92	1.73	1.84(2)
$1/2^-$	1.64	1.53	1.81(36)
$1/2^+$	1.46	–	1.76(52)

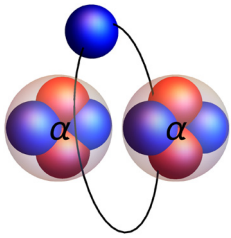

Fig. 15. Molecular-like picture of ^{9}Be, $\beta = 1.82$ fm, $\langle r^2 \rangle_\alpha^{1/2} = 1.67$ fm, $\langle r^2 \rangle_n^{1/2} = 3.53$ fm.

6. Summary and conclusions

In this article we have discussed the structure of ^{9}Be and ^{9}B within the framework of the cluster shell model (CSM) introduced in [1]. Our aim has been here: (1) to give explicitly all formulas needed for the analysis of experimental data, (2) to compare with these data, (3) to compare the results with ab initio calculations, and (4) to compare with microscopic cluster calculations. We find strong evidence for clustering in ^{9}Be and ^{9}B from energy spectra, Sect. 3.1, electromagnetic transition rates along the ground state $K^P = 3/2^-$ rotational band, Sect. 3.4.1, and longitudinal electron scattering form factors for members of the ground state $K^P = 3/2^-$ rotational band, Sect. 3.6.4.

Experimental data strongly support the structure of ^{9}Be and ^{9}B suggested by von Oertzen [17–20] implying a molecular-like picture of these nuclei, in which the last neutron (proton) acts as a binder of the two α-particles, π-binding, as shown schematically in Fig. 15.

The results of this paper suggest that clustering survives the addition of one particle. In subsequent papers we will investigate the extent to which further addition of particles as in ^{10}Be and ^{11}Be retain this result. Our calculations are in agreement with earlier calculations using the LCAO method [5–7] and the 3-body cluster calculations [21–29], but are obtained with a simpler model in which a good fraction of the results are in explicit analytic form and thus very transparent. The CSM provides a description of the observed large collective transitions without the need of introducing large $E2$ effective charges. The use of the cluster shell model introduces the needed correlations, in contrast with the spherical shell model.

Our results also provide a benchmark for comparing with ab initio calculations. Explicit comparison with the results of the Green's function Monte Carlo method (GFMC) [37] and no-core shell-model method (NCCI) [38] has been shown in Sect. 2.4 for ^{8}Be and in Sect. 3.2 and Sect. 3.5 for ^{9}Be.

Our paper provides the first and simplest step in the CSM program. The next step is the application of our method to the structure of ^{13}C, ^{13}N (D_{3h} symmetry) and ^{17}O, ^{17}F (T_d symmetry). The simplicity of our method and the fact that it can describe experimental data as accurately as fully microscopic cluster calculations is the main result of this paper and it gives confidence for the use in the more complex situations where microscopic calculations are difficult to perform.

Acknowledgements

This work was supported in part by US Department of Energy Grant No. DE-FG-02-91ER-40608 and in part by the Gran Sasso Science Institute (GSSI). We wish to thank M.A. Caprio for useful comments in the early stages of this investigation and for providing to us the results of the NCCI calculations of [38] and R. Bijker for useful comments on the spin-orbit potential.

References

[1] V. Della Rocca, R. Bijker, F. Iachello, Nucl. Phys. A 966 (2017) 158.
[2] P.D. Kunz, Ann. Phys. 11 (1960) 275;
P.D. Kunz, Phys. Rev. 128 (1962) 1343.
[3] J. Hiura, I. Shimodaya, Prog. Theor. Phys. 30 (1963) 585.
[4] V.G. Neudatchin, Yu.F. Smirnov, Prog. Nucl. Phys. 10 (1969) 275;
N.F. Golovanova, V.G. Neudatchin, Yadern. Fis. 13 (1971) 1248, Sov. J. Nucl. Phys. 13 (1971) 718.
[5] Y. Abe, J. Hiura, H. Tanaka, Prog. Theor. Phys. 49 (1973) 800.
[6] S. Okabe, Y. Abe, H. Tanaka, Prog. Theor. Phys. 57 (1977) 866.
[7] S. Okabe, Y. Abe, Prog. Theor. Phys. 61 (1979) 1049.
[8] S. Cohen, D. Kurath, Nucl. Phys. 73 (1965) 1;
T.S.H. Lee, D. Kurath, Phys. Rev. C 21 (1980) 293;
D.J. Millener, D. Kurath, Nucl. Phys. A 255 (1975) 315.
[9] A.G. Slight, T.E. Drake, G.R. Bishop, Nucl. Phys. A 208 (1973) 157.
[10] H. Feldmeier, J. Schnack, Rev. Mod. Phys. 72 (2000) 655, and references therein.
[11] R. Roth, T. Neff, H. Hergert, H. Feldmeier, Nucl. Phys. A 745 (2004) 3.
[12] T. Neff, H. Feldmeier, Nucl. Phys. A 738 (2004) 357.
[13] T. Neff, H. Feldmeier, R. Roth, Nucl. Phys. A 752 (2005) 321c.
[14] Y. Kanada-En'yo, H. Horiuchi, Prog. Theor. Phys. Suppl. 142 (2001) 205.
[15] Y. Kanada-En'yo, M. Kimura, H. Horiuchi, C. R. Phys. 4 (2003) 497.
[16] Y. Kanada-En'yo, H. Horiuchi, Phys. Rev. C 68 (2003) 014319.
[17] W. von Oertzen, Nucl. Phys. A 148 (1970) 529.
[18] W. von Oertzen, H.G. Bohlen, Phys. Rep. 19C (1975) 1.
[19] B. Imanishi, W. von Oertzen, Phys. Rep. 155 (1987) 29.
[20] W. von Oertzen, Z. Phys. A 354 (1996) 37.
[21] P. Descouvemont, Phys. Rev. C 39 (1989) 1557.
[22] K. Arai, Y. Ogawa, Y. Suzuki, K. Varga, Phys. Rev. C 54 (1996) 132.
[23] V.D. Efros, J.M. Bang, Eur. Phys. J. A 4 (1999) 33.
[24] K. Arai, P. Descouvemont, D. Baye, W.N. Catford, Phys. Rev. C 68 (2003) 014310.
[25] E. Garrido, D.V. Fedorov, A.S. Jensen, Phys. Lett. B 684 (2010) 132.
[26] R. Alvaréz-Rodriguez, A.S. Jensen, E. Garrido, D.V. Fedorov, Phys. Rev. C 82 (2010) 034001.
[27] V.D. Efros, Phys. Rev. C 89 (2014) 027301.
[28] J. Casal, M. Rodriguez-Gallardo, J.M. Arias, I.J. Thompson, Phys. Rev. C 90 (2014) 044304.
[29] M. Odsuren, Y. Kikuchi, T. Myo, M. Aikawa, K. Kato, Phys. Rev. C 92 (2015) 014322.
[30] S.C. Pieper, V.R. Pandharipande, R.B. Wiringa, J. Carlson, Phys. Rev. C 64 (2001) 014001.
[31] R.B. Wiringa, S. Piper, Phys. Rev. Lett. 89 (2002) 182501.
[32] S.C. Pieper, R.B. Wiringa, J. Carlson, Phys. Rev. C 70 (2004) 054325.
[33] S.C. Pieper, Proc. Int. School "Enrico Fermi", Course CLXIX, IOS Press, Amsterdam, 2008, p. 111, and references therein.
[34] S. Pastore, S.C. Pieper, R. Schiavilla, R.B. Wiringa, Phys. Rev. C 87 (2013) 035503.
[35] P. Navratil, J.P. Vary, B.R. Barrett, Phys. Rev. Lett. 84 (2000) 5728.
[36] P. Navratil, Proc. Int. School "Enrico Fermi", Course CLXIX, IOS Press, Amsterdam, 2008, p. 147, and references therein.
[37] P. Maris, J. Phys. Conf. Ser. 402 (2012) 012031.
[38] M.A. Caprio, P. Maris, J.P. Vary, R. Smith, Int. J. Mod. Phys. E 24 (2015) 1541002.
[39] S.G. Nilsson, Dan. Mat. Fis. Medd. 29 (16) (1955).
[40] G. Herzberg, Molecular Spectra and Molecular Structure, vol. I: Spectra of Diatomic Molecules, Krieger, Malabar, Florida, 1989.
[41] I. Sick, J.S. McCarthy, R.R. Whitney, Phys. Lett. B 64 (1976) 33.
[42] P.M. Morse, Phys. Rev. 34 (1929) 57.
[43] A.B. Volkov, Nucl. Phys. 74 (1965) 33.
[44] R. Bijker, F. Iachello, Phys. Rev. C 61 (2000) 067305.
[45] R. Bijker, F. Iachello, Ann. Phys. (N.Y.) 298 (2002) 334.
[46] R. Bijker, F. Iachello, Phys. Rev. Lett. 12 (2014) 152501.
[47] R. Bijker, F. Iachello, Nucl. Phys. A 957 (2017) 154.

[48] F. Iachello, R.D. Levine, Algebraic Theory of Molecules, Oxford University Press, Oxford, England, 1995.
[49] S. Flugge, Practical Quantum Mechanics, Springer-Verlag, Berlin, 1974.
[50] D.R. Tilley, et al., Nucl. Phys. A 745 (2004) 155.
[51] F.C. Barker, H.J. Hay, P.B. Treacy, Aust. J. Phys. 21 (1968) 239;
F.C. Barker, Aust. J. Phys. 22 (1969) 293.
[52] V.M. Daker, et al., Phys. Rev. Lett. 111 (2013) 062502.
[53] J.P. Elliott, Proc. R. Soc. A 245 (1958) 128.
[54] J.C. Bergstrom, I.P. Auer, M. Ahmad, F.J. Kline, J.H. Hough, H.S. Caplan, J.L. Groh, Phys. Rev. C 7 (1973) 2228.
[55] S. Gartenhaus, C. Schwartz, Phys. Rev. 108 (1957) 482.
[56] D.J. Rowe, Nuclear Collective Motion, World Scientific, Singapore, 2010.
[57] M.A. Preston, R.K. Bhaduri, Structure of the Nucleus, Addison–Wesley, Reading, Mass, 1975.
[58] A. De Shalit, I. Talmi, Nuclear Shell Theory, Academic Press, New York, 1963.
[59] P.J. Brussaard, P.W.M. Glaudemans, Shell-Model Applications in Nuclear Spectroscopy, North-Holland, Amsterdam, 1977.
[60] J.P. Glickman, et al., Phys. Rev. C 43 (1991) 1740.
[61] T. de Forest Jr., J.W. Walecka, Adv. Phys. 15 (1966) 1.
[62] H.G. Clerc, K.J. Wetzel, E. Spamer, Nucl. Phys. A 120 (1968) 441.
[63] J.A. Jansen, R.Th. Peerdeman, C. deVries, Nucl. Phys. A 188 (1972) 337.
[64] L. Lapikas, G. Box, H. deVries, Nucl. Phys. A 253 (1975) 324.
[65] N. Ensslin, W. Bertozzi, S. Kowalski, C.P. Sargent, W. Turchinetz, C.F. Williamson, S.P. Fivozinsky, J.W. Lightbody, S. Penner, Phys. Rev. C 9 (1974) 1705.
[66] C. Scholl, et al., Phys. Rev. C 84 (2011) 014308.
[67] V. Della Rocca, Cluster Structure of Light Luclei, Ph.D. thesis, Gran Sasso Science Institute, L'Aquila, Italy, 2017.